Trace elements and REE geochemistry of Middle Devonian carbonate mounds (Maïder Basin, Eastern Anti-Atlas, Morocco): implications for early diagenetic processes

Trace elements and REE geochemistry of Middle Devonian carbonate mounds (Maïder Basin, Eastern Anti-Atlas, Morocco): Implications for early diagenetic processes

Fulvio Franchi [a,b,*], Clara Turetta [c], Barbara Cavalazzi [d,e], Fabiana Corami [c,f], Roberto Barbieri [d]

[a] Department of Earth and Environmental Science, Botswana International University of Science and Technology, Private Bag 16, Plot 10071, Palapye, Botswana [b] ISMAR-CNR, U.O.S. Bologna, via Gobetti 101, 40129 Bologna, Italy
[c] IDPA-CNR, Institute for the Dynamics of Environmental Processes, via Torino 155, 30172, Venezia Mestre, Italy
[d] Dipartimento di Scienze Biologiche, Geologiche e Ambientali, Università di Bologna, via Zamboni 67, 40126 Bologna, Italy
[e] Department of Geology, University of Johannesburg, Kingsway PO Box 524 Auckland Park 2006, Johannesburg, South Africa
[f] DAIS Università Ca' Foscari Via Torino 155, 30172 Venezia Mestre, Italy

ARTICLE INFO

Editor: Dr. B. Jones
Keywords:
Devonian
Carbonates
Mud mounds
Diagenesis
Rare earth elements
Ce anomaly

ABSTRACT

Trace and rare earth elements (REEs) have proven their utility as tools for assessing the genesis and early diagen esis of widespread geological bodies such as carbonate mounds, whose genetic processes are not yet fully under stood. Carbonates from the Middle Devonian conical mud mounds of the Maïder Basin (eastern Anti Atlas, Morocco) have been analysed for their REE and trace element distribution. Collectively, the carbonates from the Maïder Basin mud mounds appear to display coherent REE patterns. Three different geochemical patterns, possibly related with three different diagenetic events, include: i) dyke fills with a normal marine REE pattern probably precipitated in equilibrium with seawater, ii) mound micrite with a particular enrichment of overall REE contents and variable Ce anomaly probably related to variation of pH, increase of alkalinity or dissolution/remineralization of organic matter during early diagenesis, and iii) haematite rich vein fills precipitated from venting fluids of probable hydrothermal origin. Our results reinforce the hypothesis that these mounds were probably affected by an early diagenesis induced by microbial activity and triggered by abundance of dispersed organic matter, whilst venting may have affected the mounds during a later diagenetic phase.

1. Introduction

Carbonate mounds, known in the geological record from the Proterozoic (e.g., Monty et al., 1995), are "mud dominated deposits with topographic relief and few or no stromatolites, thrombolites or in place skeletons" (Riding, 2002). Although carbonate mud mounds are mostly considered as products of diverse microbial activities (Riding, 2002), here we consider carbonate mud mounds simply as micrite dominated buildups with lack of rigid framework. Despite their fine grained texture and the absence of a rigid framework of invertebrate skeletons, carbonate mud mounds can develop into large geologic bodies with steep flanks (e.g., Brachert et al., 1992; Wendt, 1993; De Mol et al., 2005; Foubert and Henriet, 2009; Hebbeln and Samankassou, 2015).

The Devonian was a period of intensive growth of carbonate mud mounds along the north western margin of Gondwana (e.g., Dumestre and Illing, 1967; Kaufmann, 1997; Wendt et al., 1997; Wendt and Kaufmann, 2006; Franchi et al., 2014; Henriet et al., 2014). The most spectacular examples of the development of these mounds come from the Moroccan Anti Atlas (Fig. 1; Kaufmann, 1997; Franchi et al., 2014 and references therein), Western Sahara (Dumestre and Illing, 1967; Wendt and Kaufmann, 2006 and references therein), and central Algeria (Wendt et al., 1993, 1997). Mud mounds are commonly considered to typify quiet and deep marine settings (Schlager, 2003). Nevertheless, the bathymetric assessment of an ancient mound is hampered by a discontinuous fossil record and diagenesis (Hebbeln and Samankassou, 2015) that make it difficult to produce a paleoenvironmental reconstruction. The modern, deep marine mounds reported from depths between 200 m and 1000 m off the north western African coast are dominated by scleractinian cold water corals, bryo zoans and sponges (Henriet et al., 2014 and references therein) and their shape is far from being spectacular like the Devonian mounds of North Africa. Apart from these cold water, coral dominated mounds,

* Corresponding author at: Department of Earth and Environmental Science, Botswana International University of Science and Technology, Private Bag 16, Plot 10071, Palapye, Botswana.
E-mail address: franchif@biust.ac.bw (F. Franchi).

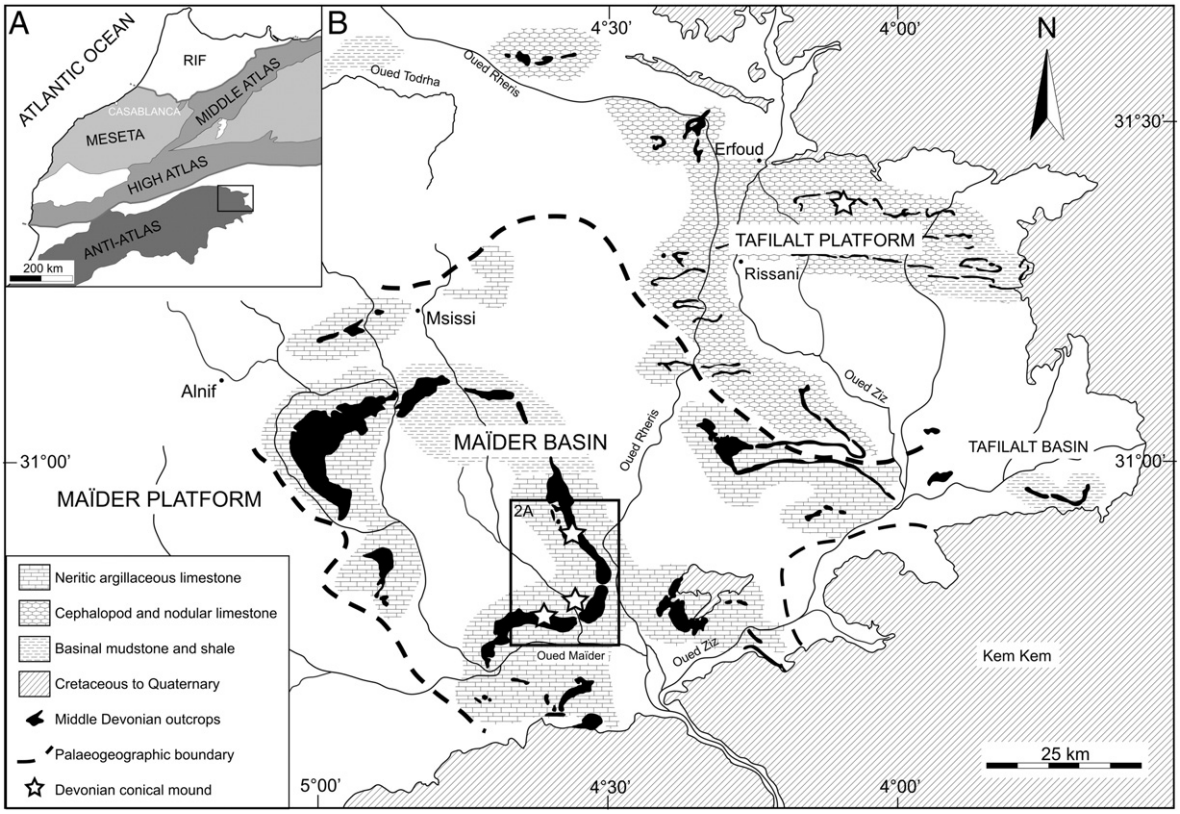

Fig. 1. A) General map of the structural domains of north-western Africa. The eastern part of Anti-Atlas domain includes (boxed area) the Devonian Tafilalt and Maïder palaeogeographic units. Modified from Michard (1976). B) Simplified geological map of the Tafilalt and Maïder platform-basin systems (boxed area in A) showing the Devonian carbonate mound occur-rences (stars). Redrawn from Kaufmann (1997).

the Phanerozoic carbonate mud mounds still lack modern analogues (Hebbeln and Samankassou, 2015).

Different conditions have been proposed for the formation of the an cient Moroccan carbonate mud mounds, including chemical precipita tion of carbonates related to anaerobic oxidation of methane (Peckmann et al., 1999, 2005; Cavalazzi, 2007; Cavalazzi et al., 2007, 2012), hydrothermal activity (Bełka, 1998; Mounji et al., 1998; Bełka and Berkowski, 2005; Franchi et al., 2014), microbial activity (Kaufmann, 1997, 1998a; Della Porta et al., 2015; Franchi et al., 2015), accumulation of coral and other macro invertebrate remains (Chafiki et al., 2004; Wendt and Kaufmann, 2006; Aretz and Herbig, 2010; Said et al., 2013). Recent assumptions that take into account strong bottom currents for the formation of small mound morphologies in the Bay of Biscay (De Mol et al., 2011) reinforce previous hypotheses (Brachert et al., 1992), suggesting the intervention of bottom currents to the for mation of the Devonian mud mounds of Hamar Laghdad (80 km north east of the Maïder Basin mounds). This theory, however, was gradually abandoned in favour of a genesis related to marine and hydro thermal fluid mixing (e.g., Bełka, 1998; Mounji et al., 1998; Franchi et al., 2014). The lack of a rigid framework suggested that eventually the me chanical processes must have been coupled with early diagenetic pro cesses that triggered the early lithification of carbonate in order to facilitate the development of steep mound flanks (Cavalazzi et al., 2007, 2012; Franchi et al., 2015; Jakubowicz et al., 2015a).

In this paper REE and other trace elements have been used to ex plore the geochemical conditions associated with the early diagenetic processes of the carbonate mounds from the Maïder Basin (MB) in the eastern Anti Atlas of Morocco (Fig. 1). They include large and solitary mounds, namely the Guelb el Maharch (GeM) and Aferdou el Mrakib (AeM), and a cluster of four mounds at Jebel el Oftal (JeO)(e.g., Kaufmann, 1997) (Fig. 2). Whilst the AeM mound has been accordingly accepted as a reef mound (Kaufmann, 1998a, 1998b; Franchi et al., 2012; Tessitore et al., 2012 and references therein), a mi crobial origin has been suggested (Kaufmann, 1997) for the micrite that mainly makes up the JeO and GeM mounds. Convincing geochemical and morphological evidences indicating a microbial mediated precipita tion of carbonates, however, are still lacking (e.g., Kaufmann, 1997, 1998a).

The rare earth elements (REEs) distribution in ancient carbonates is a powerful proxy for the reconstruction of the composition of Phanero zoic seawater (Webb and Kamber, 2000; Nothdurft et al., 2004; Shields and Webb, 2004; Johannesson et al., 2006; Olivier and Boyet, 2006) and eventual pore water conditions during formation of aqueous precipi tates (Pourret et al., 2008; Kim et al., 2012; Franchi et al., 2015). The REE geochemistry is commonly used as a proxy for the detection of i) mixing among different fluids, including seawater, freshwater and hy drothermal fluids (e.g., Kamber et al., 2004; Feng et al., 2009); ii) varia tions in seawater pH, alkalinity and redox conditions (Pourret et al., 2008; Kim et al., 2012; Hu et al., 2014) and iii) precipitation of Fe Mn oxyhydroxides (Bayon et al., 2004).

Here, we present a petrographic analysis coupled with the study of REE and trace elements distribution performed on the carbonates of the GeM mound solitary mound and, by comparison, the JeO mounds cluster (Fig. 2). Aim of this work is to better constrain the early diagen esis of GeM mound, to define the redox and alkalinity conditions during carbonate formation, and to assess the role of microbial communities during early lithification processes. The geochemical data presented here come from analyses on bulk specimens from different facies of GeM (i.e. mound limestones, stromatactis like cavities, dyke filling and veins) as well as sub samples of specific carbonate phases (micrite and cements). Bulk samples have been studied with the aim of assessing the variation in overall chemistry between the different facies. For so

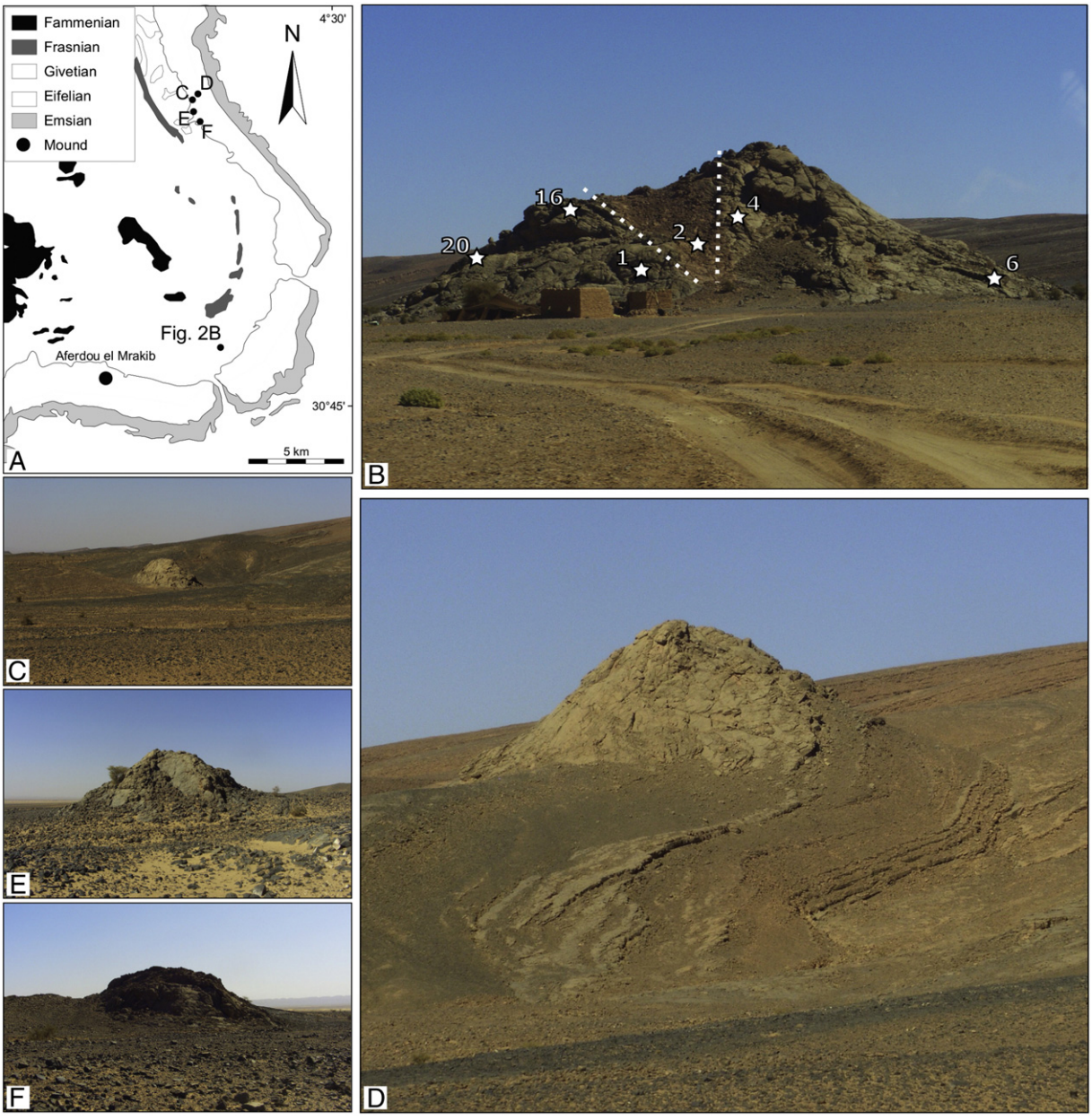

Fig. 2. A) Simplified geological map of the southern Maïder Basin (boxed area in Fig. 1B) showing the occurrences of the studied mounds (panels B–F). White area is covered by recent aeolian deposits. Outcrop views of the mounds are in panels B–F. After Kaufmann (1998b). B) Guelb el Maharch (GeM) solitary mound seen from west. The mound is dissected by a wedge of dolomitized limestones (dotted lines). The mound has a 120–180 wide exposed base and a height of *ca.* 45 m. Stars show the sampling locations (numbers refer to samples in Table 1). C–F) Jebel el Oftal (JeO) mounds (labelled as C–F in panel A). C) Mound C (mound n. 1 in Kaufmann, 1996) seen from south. It is *ca.* 50 m wide (base) and 20 m high. D) Mound D (mound n. 2 in Kaufmann, 1996) seen from south-east. It is *ca.* 40 m high. E) Mound E (mound n. 3 in Kaufmann, 1996) seen from south-east. It is *ca.* 35 m wide and 15 m high. F) Mound F (mound n. 4 in Kaufmann, 1996) seen from north. It is *ca.* 40 m wide and *ca.* 10 m high.

doing both digested samples and partial leachates have been investigat ed and compared. Eventual contamination effects are discussed. The set of analyses from sub sampled carbonatic phases, on the other hand, has been used to improve our knowledge on REE behaviour during the for mation of micrite and cement (*sensu lato*) within carbonate mud mounds and to shed light on the processes that occurs in the early stage of the mound diagenesis.

2. Geological setting & previous work

The Anti Atlas is part of the external Variscan Appalachian Ouachita Mauritanides orogen (Burkhard et al., 2006). The late Precambrian to Palaeozoic (Early Carboniferous) succession of the eastern Anti Atlas consists of a shelf sequence developed on the north western continental margin of Gondwana (Piqué and Michard, 1989; Bełka, 1998). Starting from the Devonian, the formation of the western Palaeo Tethys (Stampfli and Borel, 2002) resulted in a gradual formation of the Tafilalt and Maïder intracratonic sedimentary platform basin systems (Wendt, 1985; Baidder et al., 2016 for review).

The studied Devonian mounds crop out along a *cuesta* of Devonian rocks in the MB, located *ca.* 50 km south of the village of Msissi (Figs. 1, 2A). The carbonate mounds are exposed on top of a 200 300 m thick Middle Devonian succession of fossiliferous, argillaceous limestone (Hollard, 1974; Wendt, 1993; Döring and Kazmierczak, 2001). These mounds consist of stromatactis bearing wackestone, floatstone and packstone/grainstone and have overall conical shape and dimension similar to the Early Devonian (Emsian) Kess Kess mounds in the Tafilalt Platform (e.g., Brachert et al., 1992). Only the

AeM mound is likely placed within the photic zone retaining reef char acteristics with a convincing reef faunal association (Kaufmann, 1997, 1998a, 1998b; Franchi et al., 2012; Tessitore et al., 2012), whereas the other mounds display similar faunal assemblages a dominance of crinoids, trilobites, tabulate corals (mainly auloporids), and brachiopods suggesting a depositional environment placed well below the euphotic zone (Wendt, 1993; Kaufmann, 1995, 1997; Jakubowicz et al., 2015b). On the basis of the high $\delta^{18}O$ values yielded by early marine cements, these mounds were previously assigned to environmental conditions characterized by cold and deep waters (Kaufmann, 1997). This reconstruction, however, seems contrary to the recovery of remains of phototrophic bacteria in stromatactis cavities of MB mounds (Kaufmann, 1998a). Following the description of the phototrophic remains, an overall microbial origin for the micrite of the MB mounds (Kaufmann, 1998a) appears plausible. The more so considering the nearly pure carbonate composition (95% $CaCO_3$, Kaufmann, 1996) of the mounds carbonate that suggests an authigenic origin. Nevertheless, the origins of the four mounds exhumed at the JeO (from C to F in Fig. 2) and GeM (solitary mound, Fig. 2B) are still debated. Because of their alignment along a Precambrian, E W trending strike slip fault system (Kaufmann, 1998a), some hydrothermal fluid circulation was the al leged triggering factor for the early lithification of carbonates of the AeM and GeM mounds (Kaufmann, 1996, 1998a). Although the $\delta^{18}O$ values measured in the MB mounds (Kaufmann, 1997) do not convincingly support a fault controlled seepage of fluids and/or hydrothermal venting, some contribution by low temperature fluid advection to the mounds cannot be excluded (Kaufmann, 1998a).

3. Material and methods

A total of 20 samples from the different facies of GeM and JeO mounds (Figs. 1 2) were analysed for mineralogical and chemical composition (Tables 1 2). Considering its clear reefal origin, the abundance of frame builders and the different scale (hundreds of meters) the AeM mound has been excluded from the present study which is focused on the alleged microbial and/or hydrothermal related mounds. The petro graphic and microfacies analyses were performed using standard petro graphic thin sections. Cathodoluminescence microscopy was conducted using a CITL 8220 MK3 instrument (operating conditions: 20 kV beam voltage and 200 μA beam current) at the University of Torino. Morpho logical and elemental analyses of the studied samples were obtained using a Jeol 5600 Scanning Electron Microscope (SEM) equipped with an electron back scattering CENTAURUS system and energy dispersive X ray spectrometry (EDS) at the University of Johannesburg. SEM EDS investigations were performed on freshly broken samples as well as polished thin sections and epoxy mounts (operating conditions:

Table1
Summary of carbonate samples and sub-samples (in grey) investigated in the Maïder Basin.

N.	Sample description	Mineralogical composition[a]	Facies	Phase analysed	Mound	
1	Grey wackestone	High–Mg calcite (dolomite)	Mound	Bulk	Guelb el Maharch	
2	Saccharoidal dolostone	Calcite, Dolomite	Dolomitized limestones	Bulk		
4	Black and purple banded limestone	Calcite	Vein filling	A) Dark grey micrite		
		Calcite		B) Reddish micrite		
6	Brachiopod/crinoid floatstone		Mound	Grey micrite		
8	Yellow wackestone with trilobite remains	Calcite, quartz	Cavity	Bulk		
8	Yellow wackestone with trilobite remains	Calcite, quartz	Cavity	A) Yellow micrite		
		Calcite, quartz	Cavity	B) Cements		
9	Brachipod floatstone	Calcite	Mound	Grey micrite		
10	Dark Grey banded limestone	Calcite	Dyke	Dark banded mudstone		
11	Grey wackestone with stromatactis	Calcite	Mound	A) Grey micrite		
		Calcite		B) Stromatactis fill (cements)		
13	Dark grey limestone	Calcite	Dyke	Bulk		
13	Dark grey limestone	High–Mg calcite	Dyke	A) Light grey micrite		
		Calcite	Dyke	B) Dark grey micrite		
14	Black and purple banded limestone	Calcite	Vein filling	A) Wackestone		
		Calcite, hematite		B) Red micrite		
				C) Withish part		
15	Black and purple banded limestone	Calcite, hematite	Vein filling	Bulk		
16	Grey wackestone	Calcite	Mound	Micrite (avoid big crinoids)		
20	Grey wackestone	High–Mg calcite (dolomite)	Mound	Bulk		
33	Trilobite floatstone/rudstone	Calcite	Cavity	Bulk		Jebel el Oftal
33	Trilobite floatstone/rudstone	Calcite	Cavity	A) Dark micrite	4	
	Trilobite floatstone/rudstone	Calcite	Cavity	B) Cements		
34	Grey wackestone	High–Mg calcite	Mound	Bulk		
35	Trilobite and coral floatstone/rudstone	Calcite	Cavity	Bulk	3	
35	Trilobite and coral floatstone/rudstone	Calcite	Cavity	A) Cements		
		Calcite	Cavity	B) Micrite		
38	Grey grainstone with stromatactis	Calcite	Cavity	A) Crinoid/coral grainstone		
		High–Mg calcite	Cavity	B) Cements	2	
39	Grey floatstone	Calcite	Mound	A) Micrite		
				B) Cements		
40	Grey wackestone	High–Mg calcite	Mound	Bulk	1	
41	Grey wackestone	High–Mg calcite, quartz	Mound	Bulk		

[a] Based on XRD data integrated with EDS analyses.

Table 2
PAAS-normalized REE concentrations (ppm), calculated parameters, ratios, Mo, Th and U concentrations (ppm) for the studied bulk samples (in white) and sub-samples (in grey).

Samples	1	2	4–A	4–B	6	8	8–A	8–B	9	10	11–A	11–B	13	13–A	13–B	14–A	14–B	14–C	15	16	20	33	33–A	33–B	34	35	35–A	35–B	38–A	38–B	39A	39–B	40	41
La	0.079	0.157	0.071	0.240	0.072	0.112	0.137	0.074	0.082	0.042	0.083	0.034	0.059	0.040	0.055	0.109	0.008	0.023	0.054	0.259	0.024	0.099	0.144	0.018	0.054	0.065	0.027	0.123	0.078	0.032	0.070	0.081	0.102	0.082
Ce	0.055	0.096	0.066	0.183	0.053	0.064	0.091	0.029	0.080	0.037	0.064	0.020	0.037	0.036	0.032	0.233	0.008	0.023	0.042	0.180	0.017	0.069	0.107	0.012	0.124	0.031	0.020	0.098	0.078	0.024	0.041	0.033	0.104	0.066
Pr	0.092	0.203	0.072	0.204	0.079	0.107	0.142	0.049	0.104	0.051	0.096	0.038	0.047	0.047	0.045	0.105	0.008	0.020	0.053	0.317	0.028	0.105	0.156	0.016	0.065	0.063	0.029	0.136	0.092	0.031	0.068	0.070	0.125	0.096
Nd	0.110	0.261	0.075	0.203	0.089	0.130	0.163	0.055	0.120	0.059	0.110	0.045	0.048	0.061	0.053	0.113	0.009	0.023	0.064	0.369	0.032	0.119	0.171	0.017	0.075	0.072	0.032	0.148	0.103	0.036	0.074	0.077	0.146	0.111
Sm	0.143	0.414	0.096	0.258	0.122	0.170	0.222	0.070	0.167	0.082	0.144	0.064	0.060	0.092	0.069	0.150	0.007	0.026	0.095	0.544	0.047	0.141	0.210	0.021	0.103	0.095	0.043	0.183	0.133	0.044	0.089	0.097	0.190	0.145
Eu	0.178	0.490	0.115	0.313	0.132	0.221	0.282	0.094	0.208	0.098	0.161	0.079	0.092	0.118	0.086	0.177	0.009	0.038	0.136	0.656	0.068	0.173	0.237	0.029	0.136	0.129	0.051	0.205	0.147	0.056	0.099	0.118	0.225	0.180
Gd	0.203	0.604	0.124	0.315	0.149	0.256	0.280	0.123	0.194	0.108	0.172	0.088	0.092	0.140	0.106	0.196	0.011	0.041	0.155	0.710	0.069	0.190	0.257	0.034	0.135	0.146	0.063	0.224	0.161	0.069	0.123	0.148	0.239	0.191
Tb	0.179	0.499	0.122	0.240	0.133	0.220	0.241	0.110	0.163	0.092	0.148	0.079	0.096	0.115	0.092	0.175	0.006	0.033	0.145	0.611	0.073	0.167	0.219	0.029	0.126	0.140	0.058	0.187	0.142	0.059	0.107	0.142	0.207	0.164
Dy	0.161	0.447	0.121	0.207	0.131	0.209	0.229	0.125	0.147	0.091	0.141	0.080	0.086	0.115	0.094	0.167	0.009	0.034	0.135	0.565	0.054	0.148	0.215	0.033	0.102	0.128	0.062	0.179	0.137	0.063	0.109	0.154	0.180	0.140
Ho	0.159	0.374	0.124	0.183	0.127	0.216	0.227	0.145	0.134	0.089	0.136	0.084	0.098	0.116	0.096	0.164	0.006	0.034	0.144	0.530	0.063	0.153	0.217	0.035	0.108	0.142	0.064	0.178	0.133	0.064	0.113	0.167	0.176	0.142
Er	0.137	0.296	0.123	0.154	0.124	0.198	0.214	0.154	0.122	0.086	0.129	0.082	0.089	0.113	0.095	0.155	0.007	0.032	0.131	0.477	0.049	0.134	0.213	0.036	0.089	0.127	0.065	0.173	0.128	0.064	0.111	0.169	0.152	0.122
Tm	0.128	0.215	0.118	0.113	0.103	0.178	0.182	0.132	0.097	0.071	0.103	0.067	0.100	0.093	0.074	0.144	0.000	0.021	0.130	0.385	0.068	0.133	0.178	0.029	0.102	0.131	0.052	0.145	0.107	0.044	0.091	0.140	0.147	0.123
Yb	0.108	0.176	0.108	0.096	0.101	0.160	0.162	0.123	0.090	0.069	0.097	0.063	0.082	0.086	0.063	0.125	0.001	0.019	0.113	0.336	0.041	0.110	0.164	0.028	0.072	0.105	0.048	0.134	0.099	0.041	0.084	0.130	0.124	0.099
Lu	0.116	0.157	0.104	0.078	0.090	0.166	0.154	0.116	0.078	0.061	0.087	0.057	0.098	0.075	0.055	0.121	0.000	0.015	0.120	0.298	0.065	0.124	0.151	0.025	0.094	0.123	0.044	0.121	0.090	0.033	0.077	0.115	0.135	0.114
Y			0.187	0.303	0.199		0.383	0.403	0.190	0.158	0.225	0.171		0.247	0.189	0.256	0.024	0.079		0.787			0.405	0.088			0.134	0.327	0.241	0.166	0.237	0.358		
Y/Ho			41.3	45.2	42.6		46.0	75.9	38.6	48.7	45.0	55.9		58.2	53.5	42.5	107.6	62.8		40.5			50.9	68.9			57.1	50.2	49.2	70.4	57.3	58.4		
ΣREE	15.5	33.5	13.9	37.8	13.8	19.3	24.8	10.2	18.2	9.1	16.2	6.6	9.1	9.5	8.9	31.4	1.5	4.4	10.9	52.8	4.9	17.6	26.4	3.1	17.5	10.7	5.3	23.1	16.7	6.0	11.5	12.3	22.4	16.2
La/La*	1.25	1.27	1.05	1.16	1.17	1.53	1.25	1.88	1.06	1.09	1.13	1.32	1.30	1.39	1.66	1.18	1.22	1.42	1.50	1.11	1.12	1.21	1.11	1.46	1.08	1.34	1.20	1.07	1.07	1.38	1.21	1.36	1.11	1.14
Ce/Ce*	0.72	0.61	0.94	0.89	0.76	0.72	0.73	0.67	0.89	0.84	0.76	0.63	0.80	0.96	0.82	2.37	1.11	1.28	0.97	0.66	0.71	0.75	0.75	0.83	2.17	0.56	0.79	0.78	0.95	0.87	0.66	0.51	0.97	0.79
Eu/Eu*	1.15	1.11	1.11	1.25	1.05	1.19	1.24	1.15	1.26	1.14	1.11	1.16	1.31	1.18	1.14	1.12	1.45	1.34	1.25	1.16	1.24	1.16	1.11	1.27	1.23	1.19	1.08	1.11	1.08	1.15	1.05	1.07	1.15	1.19
Gd/Gd*	1.17	1.26	1.02	1.38	1.13	1.18	1.18	1.07	1.24	1.18	1.19	1.11	1.00	1.22	1.15	1.14	1.54	1.24	1.10	1.19	1.05	1.18	1.18	1.12	1.15	1.07	1.06	1.21	1.15	1.15	1.14	1.01	1.21	1.22
Pr/Yb	0.85	1.16	0.67	2.13	0.78	0.67	0.88	0.40	1.16	0.74	0.99	0.60	0.58	0.55	0.72	0.84	6.18	1.06	0.47	0.94	0.69	0.96	0.95	0.56	0.91	0.60	0.59	1.02	0.93	0.76	0.81	0.54	1.01	0.97
Pr/Tb	0.51	0.41	0.59	0.85	0.59	0.49	0.59	0.45	0.64	0.55	0.65	0.48	0.49	0.41	0.50	0.60	1.27	0.61	0.37	0.52	0.39	0.63	0.71	0.55	0.52	0.45	0.49	0.73	0.65	0.53	0.64	0.50	0.60	0.58
Tb/Yb	1.66	2.84	1.13	2.50	1.32	1.37	1.49	0.90	1.81	1.33	1.52	1.25	1.17	1.34	1.45	1.40	4.88	1.73	1.28	1.82	1.77	1.52	1.34	1.03	1.75	1.34	1.20	1.40	1.43	1.44	1.27	1.09	1.67	1.65
Mo	0.042	0.064	0.006	u.d.l.	0.007	0.039	0.003	0.002	0.016	0.015	0.027	0.003	0.049	0.010	u.d.l.	0.011	u.d.l.	u.d.l.	0.034	0.009	0.030	0.048	0.024	0.016	0.066	0.036	0.008	0.021	0.013	0.005	0.015	0.086	0.057	0.036
Th	0.023	0.131	0.073	0.216	0.345	0.050	0.390	0.013	0.589	0.136	0.462	0.097	0.069	0.016	u.d.l.	0.190	0.001	0.009	0.113	0.823	0.024	0.034	0.537	0.007	0.020	0.020	0.011	0.563	0.566	0.030	0.287	0.049	0.022	0.027
U	0.582	0.253	0.019	0.076	0.025	0.459	0.021	0.034	0.016	0.071	0.016	0.005	0.027	0.164	0.017	0.014	0.247	0.057	0.179	0.019	0.150	0.551	0.009	0.021	0.522	0.174	0.018	0.015	0.012	0.014	0.015	0.071	0.759	0.587

15 and 25 kV accelerating voltage). X ray diffraction (XRD) analyses (Table 1) were performed with a Bruker D8 Advance X ray diffractometer (Cu Kα X ray source) at Botswana International University of Science and Technology (BIUST).

11 samples for preliminary geochemical analyses were obtained from bulk rocks (Tables 1, 2). Specific carbonate phases have been identified during petrographic analyses and selected for finer sub sampling (23 samples, grey in Tables 1, 2). Trace element compositions were analysed by inductively coupled plasma quadrupole mass spectrometry (ICP QMS) on acid leachates using an Agilent 7500 fitted with a standard double pass spray chamber and v groove nebulizer (RF power 1400 W, sample gas 1.20 μL min^{-1}, sample flow rate 500 μL min^{-1}, dwell time 20 ms, 3 points per peak), at the Institute for the Dynamics of Environmental Processes Consiglio Nazionale delle Ricerche (IDPA CNR) of Venice. Two sets of analyses were performed on i) bulk rock and ii) sub sampled carbonatic phases (Table 2). For the bulk rock anal- yses, *ca.* 300 mg of sample was leached with 5% ultrapure acetic acid (CH_3COOH) for 1 h. Insoluble residue was separated by centrifuging and then mineralized in a microwave oven (Milestone MLS 1200 Mega- microwave laboratory unit) using an acid mixture (6 mL HNO_3 and 4 mL HF) to solubilize the entire residue. In addition, *ca.* 300 mg of bulk sample was also subjected to acid digestion (using a mixture of 9 mL HNO_3, 4 mL HF and 2 mL H_2O_2) in the microwave oven to obtain total dissolution. Leached and mineralized samples were diluted 10 times with ultrapure water (Pure Lab Ultra Water System Elga Lab Water, High Wycombe, UK) and then analysed. Then the results of total dissolution were compared with those of partial dissolutions (carbonate phases and insoluble residuum), and this led to an evalua- tion of the accuracy of the analyses (see Supplementary materials S1). For the analyses of specific sub sampled carbonate phases, *ca.* 300 mg of sample was leached with 2% ultrapure acetic acid following the pro- tocol proposed by Rongemaille et al. (2011). The accuracy of the mea- surements was determined using two certified reference materials (CRM MESS3, a marine sediment, and BCR 667, an estuarine sediment) in which the trace element concentrations were measured. The accura- cy of measurements (expressed as a relative percent error Er%) was between 0.03 and 8.8%, except for Cd and Zn (13.3 and 16.9%, respec- tively), in BCR 667 and between 0.7 and 12.5% (Zn and Se show higher value of Er: 16.7 and 18.9% respectively) in MESS3. The precision of measurements, expressed as a percentage relative standard deviation (RSD %) calculated on six repetitions, was between 0.7 and 13.3% (see Supplementary materials S2). LOD (the instrumental signal of the pro cedural blank ± 3 times the standard deviation of the procedural blank) and LOQ (the instrumental signal of the procedural blank ± 10 times the standard deviation of the procedural blank) were calculated (see Supplementary materials S2). For all the trace elements and the REE analysed the instrumental signal of the sample was always above LOQ. Trace elements and REE contents of the totally leached sample, carbonate phases and insoluble residuum from bulk rock analyses are re ported in the supplementary materials (Supplementary materials S2).

The relative abundances of REE were normalized to Post Archean Australian Shale (PAAS, Taylor and McLennan, 1985) representing an estimate for the composition of average terrigenous input to the oceanic environment (Table 2). We calculated ΣREE, La, Ce, Eu and Gd anomalies (Table 2) and the relation between these proxies and trace and transition elements for the carbonate phases. REE fractionation was calculated as Pr_{SN} / Yb_{SN} (SN, shale normalized) to avoid problems in case of anomalous La and Ce concentrations (Table 2). LREE *vs* MREE and MREE *vs* HREE enrichments were calculated as Pr_{SN} / Tb_{SN} and Tb_{SN} / Yb_{SN}, respectively (Table 2). In order to avoid any anomalous behaviour of La, Ce, Eu and given the quasi linear behaviour of the near neighbour REE in the logarithmic plots (see below), the anomalies were calculated using the geometric equation given by Lawrence et al. (2006):

$$La/La^* \quad [La/(Pr^*(Pr/Nd)^2]_{SN} \tag{1}$$

$$Ce/Ce^* \quad [Ce/(Pr^*(Pr/Nd)]_{SN} \tag{2}$$

$$Eu/Eu^* \quad \left[Eu/\left(Sm^2 * Tb\right)^{1/3}\right]_{SN} \tag{3}$$

$$Gd/Gd^* \quad \left[Gd/\left(Tb^2 * Sm\right)^{1/3}\right]_{SN} \tag{4}$$

To better constrain the variations of palaeoredox conditions within the MB limestones, U_{EF} and Mo_{EF} (EF, enrichment factors) of the bulk rocks have been calculated (Table 3). We used the equations given by Hu et al. (2014):

$$X_{EF} \quad \left[(X/Al)_{sample}/(X/Al)_{reference}\right] \tag{5}$$

where X and Al represent the concentrations of the elements X and the weight concentrations of Al (ppm). Samples were normalized using the Earth's upper crust compositions (McLennan, 2001).

4. Mounds and samples description

Detailed facies analyses of the MB mounds are provided in Kaufmann (1995, 1996, 1997, 1998a, 1998b). The following chapter is a summary of sedimentological and stratigraphic aspects revealed during field mapping carried out in 2011 by FF and considered useful for a discussion on the GeM mound (Fig. 2).

4.1. Guelb el Maharch (GeM) mound

This early Givetian, 45 m high mound (Fig. 2B) emerges with an elliptical shape (approx. 120 by 180 m) from the south eastern margin of the study area (Figs. 1, 2A). The bulk of this mound consists of wackestone/floatstone dominated by crinoids, tabulate corals, and tentaculites (Figs. 3A B, 4A B). The limestone of the GeM mound is typified by stromatactis (Fig. 3C E) filled with isopachous generations of turbid (inclusion rich) and fibrous, radiaxial calcite (Fig. 4A) and blocky calcite.

The GeM mound is dissected by a wedge of reddish, dolomitized limestone (Fig. 2B) characterized by zoned euhedral dolomite (Figs. 4C D, 5A B), and by two systems of fractures (Fig. 3F H). The first system, referred to as neptunian dykes (Kaufmann, 1998a), is filled by layered micrite and microsparite, sparry cements, portions of the overlying strata and brachiopod shells (Fig. 3F G). The layered micrite (Table 1) consists of a clotted fabric typified by amalgamated peloids and spar filled cavities (Fig. 4E F). Other fractures (hereafter refers to as 'veins') are filled by dark to purple, banded material cementing lithoclasts and nodules of iron bearing micrite (Fig. 3H). The vein fill consists of an alternation of opaque hematite (Table 1) and fenestral, brownish microsparite (Figs. 4G, 5C D) with internal layering due to

Table 3
Mo and U enrichment factors, total REE content, and Fe distribution of bulk carbonate samples.

Sample	Al (ppm)	Mo_{EF}	U_{EF}	Mo_{EF}/U_{EF}	ΣREE	ΣREE/Fe
1	25.69	87.49	25.15	3.48	15.46	0.021
2	196.75	17.53	19.08	0.92	33.46	0.015
8	91.53	22.97	15.80	1.45	19.29	0.016
13	12.83	204.94	153.49	1.34	9.15	0.007
15	151.64	12.08	21.33	0.57	10.94	0.002
20	12.24	132.09	55.28	2.39	4.90	0.013
33	29.05	88.43	33.17	2.67	17.60	0.013
34	47.55	74.73	12.31	6.07	17.47	0.018
35	16.07	119.31	34.86	3.42	10.70	0.015
40	92.80	32.92	6.93	4.75	22.39	0.014
41	105.95	18.20	7.31	2.49	16.24	0.012

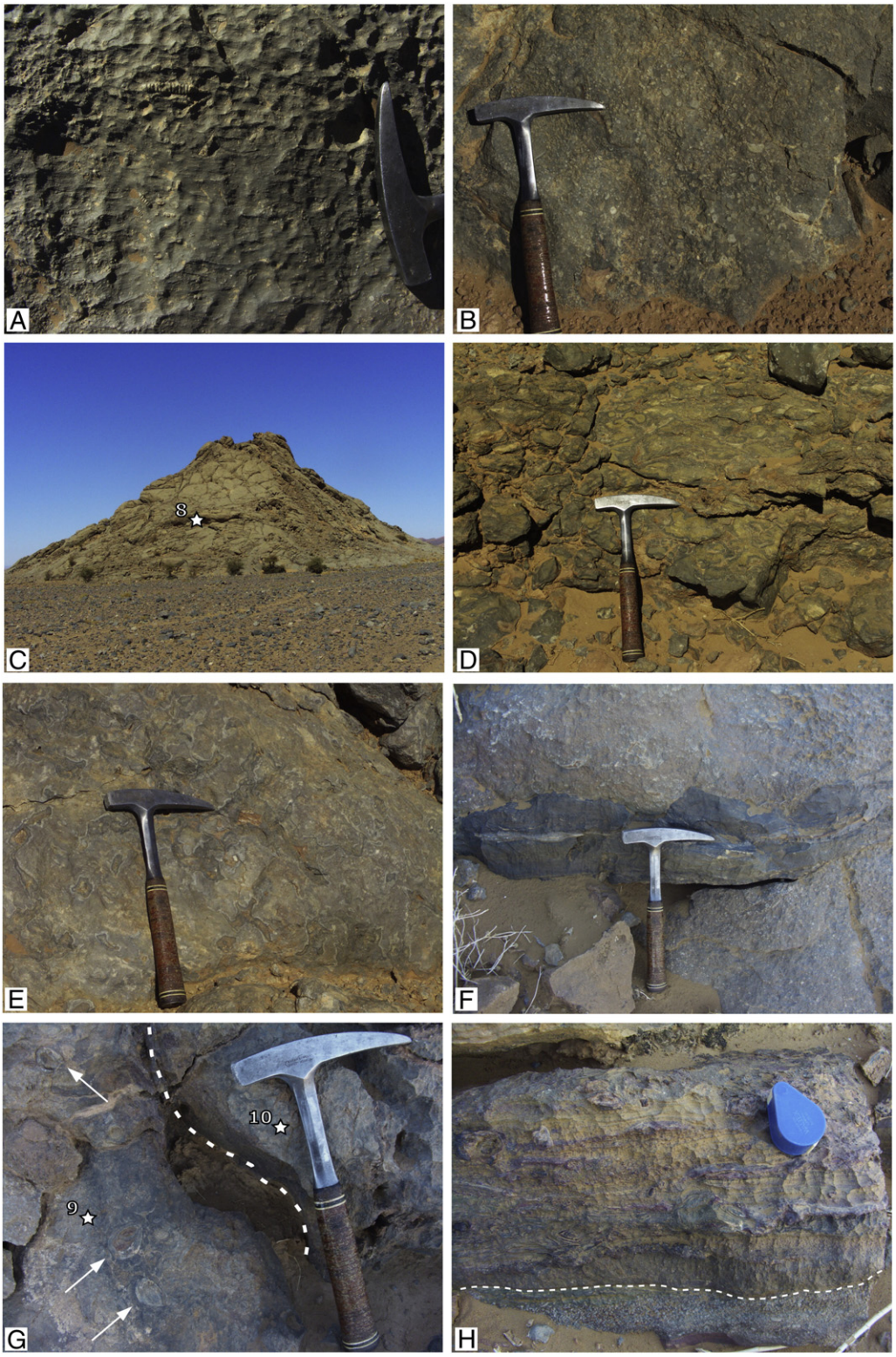

Fig. 3. Guelb el Maharch (GeM) outcrop views. A) Grey wackestone with sparse large crinoid remains (sample 1). See Fig. 2B for sampling site location. B) Brachiopod/crinoid floatstone (sample 6). See Fig. 2B for sampling site location. C) GeM southern flank showing the location of sample 8 (D). E) Stromatactis-bearing limestone (sample 11). F) Horizontal neptunian dyke filled by dark grey limestones (sample 13). G) Close-up of a sub-vertical neptunian dyke (dotted line indicates the contact with grey crinoid wackestone to the right) filled by dark limestones, lithoclasts, and articulated brachiopods (arrows). Stars show the location of samples 9 and 10. H) Horizontal vein filled by banded grey limestones and purple hematite-rich layers (samples 14 and 15). The base of the fracture (dotted line) shows a dense accumulation (grainstone) of crinoid ossicles.

alternation of peloidal and fenestral fabric. The walls of both veins and dykes consist of crinoid grainstone and brachiopod floatstone (Fig. 3F H). Brachiopod shells, in particular, are overgrown by syntaxial calcite and scalenohedral cements and are often dissected by pressure dissolution structures (Fig. 4H). Articulated brachiopod shells from the neptunian dykes mainly belong to atrypids (*Desquamatia*?) and

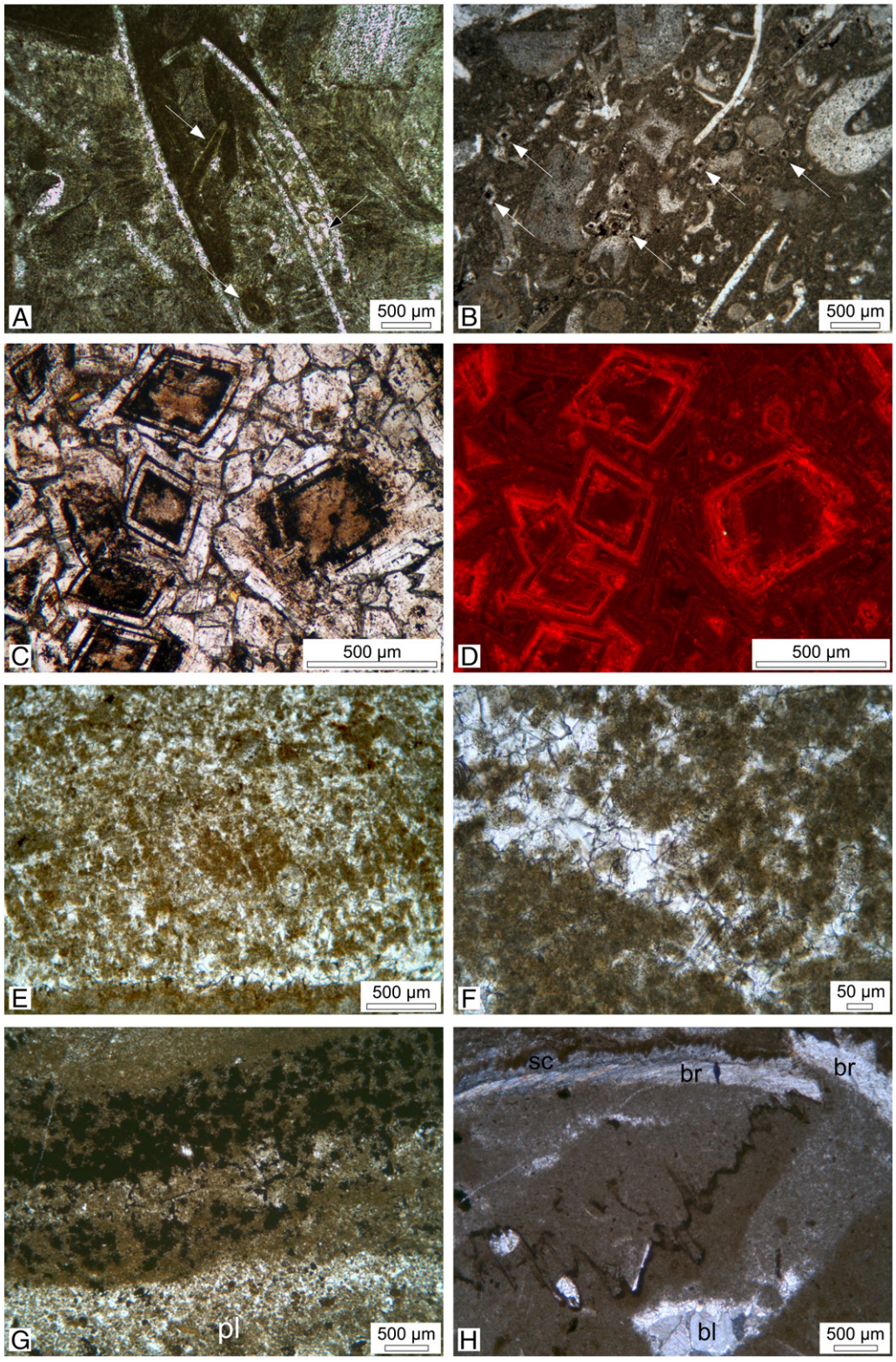

Fig. 4. Photomicrographs of the Guelb el Maharch (GeM) mound carbonate rocks. A) Stromatactis fill (sample 8): micrite roof (top), fibrous radiaxial calcite, scalenohedral calcite (black arrow). Bioclasts are mainly crinoids (up right corner), brachiopod remains, and tentaculites (white arrows). B) Crinoid wackestone (sample 20). Arrows point to sub-euhedral dolomite crystal. Note the preferential dolomitization of micrite. C) Euhedral rhombohedra of dolomite from the dolomitized limestone wedge of the GeM mound (sample 2). Dolomite rhombohedra show zonation of calcite (see also Fig. 5). Bulk of the rock consists of mosaic made of idiotopic euhedral to sub-euhedral dolomite crystals (in D). D) Idiotopic dolomite, same as C, under cathodoluminescence. E) Peloidal fabric of the layered micrite filling the neptunian dykes (sample 13). F) Close up of E showing the rounded shape of the peloids and the spar-filled cavities. Note that peloids are rich in micro-inclusions of dark opaque minerals. G) Layering within a vein fills showing alternation of peloidal micrite (pl) and fenestral micrite. Note the fenestrae totally filled by opaque material (see also Fig. 5C–D). H) Brachiopod (br) rudstone. Note the scalenohedral cement (sc) overgrowth on brachiopod shell. Voids are filled with blocky calcite (bl). Note the pressure-dissolution structures that cut across the section.

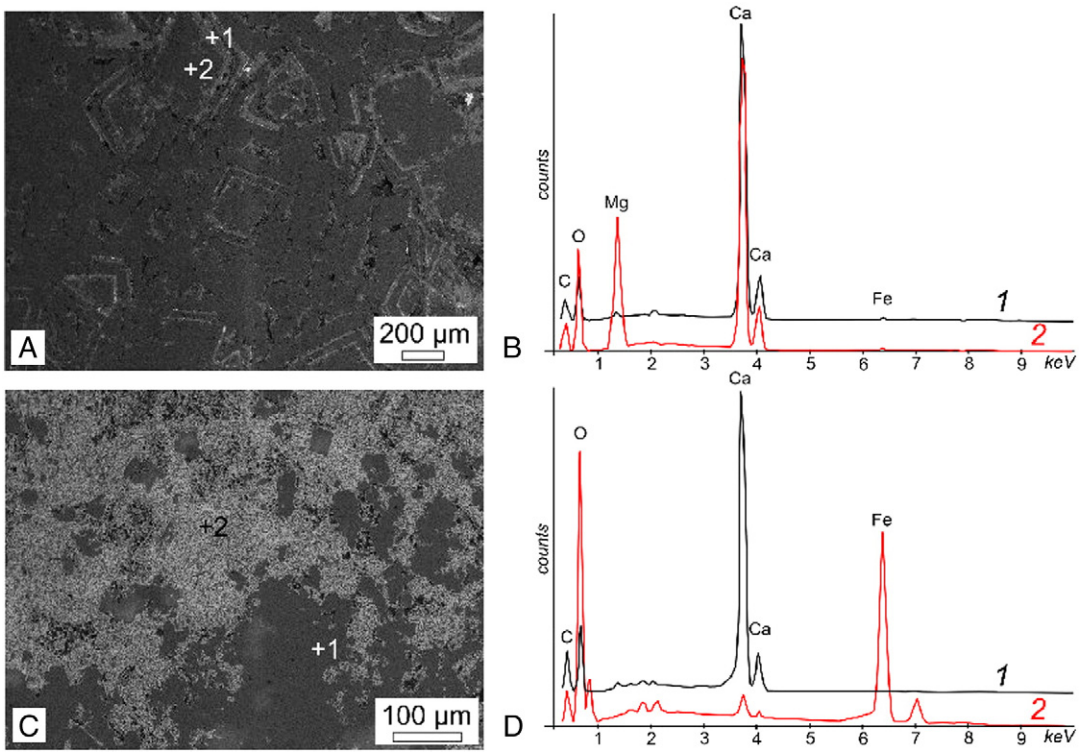

Fig. 5. Backscattered electrons images (BEI) and EDS spectrum of fracture infills. A) Idiotopic dolomite from sample 2. B) EDS spot analyses of dolomite mosaic in A. 1: calcite; 2: dolomite. C) Vein infill (sample 15). D) EDS spot analyses of sample 15. 1: calcite; 2: hematite (see Table 1).

rhynchonellid (*Camarotoechia marocanensis*; Schemm Gregory pers. comm., 2012). Atrypids (*Desquamatia*?) are also common in the AeM reef mound and their occurrence is consistent with the Givetian age (Lower *varcus* zone) proposed by Kaufmann (1997), whereas the occurrence of *C. marocanensis* within fracture fills may suggest a younger age, probably between upper Givetian and lower Frasnian (Biernat and Szulczewski, 1975; Sartenaer, 1994). This faunal mixing might be related to formation of neptunian dykes and their conse quent dykes filling with the Givetian sediments that overlie the car bonate buildup.

4.2. Jebel el Oftal (JeO) mounds

The four mounds of the JeO are early to late Eifelian in age (Kaufmann, 1997). In this paper their numbering follows the one proposed by Kaufmann (1996) from 1 to 4 (Fig. 2C, D, E and F, respectively). These mounds have an asymmetric shape and are partially covered by more recent deposits (Fig. 2C, E). The bulk of the mounds consists of stromatactis bearing wackestone/floatstone with abundant skeletal (crinoid, trilobite, coral, and rare brachiopod) components (Fig. 6). Coral primary porosity is filled by blocky and syntaxial calcite. Millimetre wide dykes are lined by isopachous generation of marine cements (i.e. fibrous radiaxial calcite), shallow burial cements (i.e. scalenohedral and bladed calcite) and filled by micrite (Fig. 7A B). Decimetre to metre sized stromatactis like cavities filled by trilobite bearing (phacopids and scutellids) floatstone/rudstone occur in mounds 2 and 4 (Fig. 7C D). Analogue cavities have been described from GeM. Bright luminescent micrite and trilobite remains are over grown by a first generation of dull luminescent, scalenohedral calcite that grades into banded luminescent calcite and bladed calcite (Fig. 7D).The bladed crystals show smooth terminations probably due to dissolution effects (see discussion below). Toward the centre of the vugs between the skeletal remains there are several generations of bright and dull luminescent fibrous radiaxial calcite. The latest generations of cements are non luminescent blocky calcite and syntaxial calcite (Fig. 7D).

5. Results

5.1. Carbonate geochemistry

5.1.1. Mineralogical composition

XRD analyses revealed that samples from the different mound facies consist of both low and high Mg calcite with subordinate amounts of dolomite and quartz (Table 1). Particularly, stromatactis like cavity fills reveal traces of quartz. Dolomite is pervasively present in the mounds facies, as protodolomite (Fig. 4B) or hypidiotopic mosaic of euhedral crystals (Figs. 4C D, 5A B). The layered micrite from dyke fills of the GeM mound consists of high Mg calcite, whilst the banded red/purple rock that fills the veins mainly consists of hematitized calcite (Table 1, Fig. 5C D).

5.1.2. Trace elements and REE geochemistry

Eleven samples have been investigated for their bulk geochemical composition. Trace elements and REE distributions have been investigated within the total digested sample as well as within carbonate leachate (weak acid leaching) and insoluble residuum. The complete re sults are reported in the supplementary materials (Supplementary ma terials S1). Table 2 shows REE and selected trace elements distribution from the carbonate leachates. Elements such as Rb and Th show a low generalized concentration in the carbonate leachate (0.02 0.25 ppm and 0.03 0.76 ppm, respectively). Iron content in the carbonate leach ate ranges between 379.87 ppm and 4172.12 ppm, with higher concen trations within the vein and dyke fills and in the wackestone collected from JeO (mound 1). Mn content ranges between 145.70 ppm and 1178.67 ppm. The concentrations of Mo and U range from 0.03 to

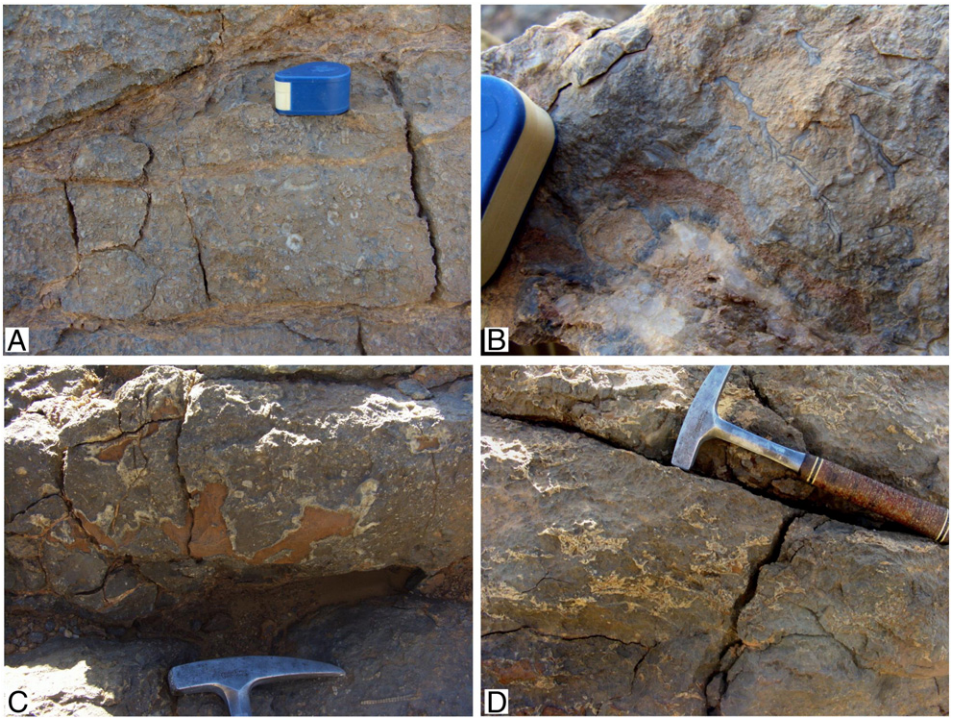

Fig. 6. Jebel el Oftal (JeO) mounds outcrop views. A) Grey crinoid wackestone/floatstone forming the bulk of the mounds (samples 40, 41). Photograph shows the basal strata of mound n. 1 (Fig. 2C). B) Mound n. 2 (Fig. 2D): large corals within stromatactis (bottom) bearing crinoidal wackestone/grainstone (sample 38). C) Stromatactis-bearing crinoid floatstone (sample 35). Photograph shows the apical part of mound n. 3 (Fig. 2E). D) Mound n. 4 (Fig. 2F): spar-filled stromatactis (sample 33).

0.07 ppm and from 0.02 to 0.13 ppm, respectively (Table 2). REE patterns of bulk rock samples from GeM and JeO (Table 2) are reported in Fig. 8. The ΣREE ranges between 1.5 ppm, in the hematite rich vein fills, and 52.8 ppm, in the GeM mound micrite (Table 2). Geochemical analyses on the bulk samples of limestone from GeM revealed quite homogeneous REE pattern among the mound facies (Fig. 8A). All but one

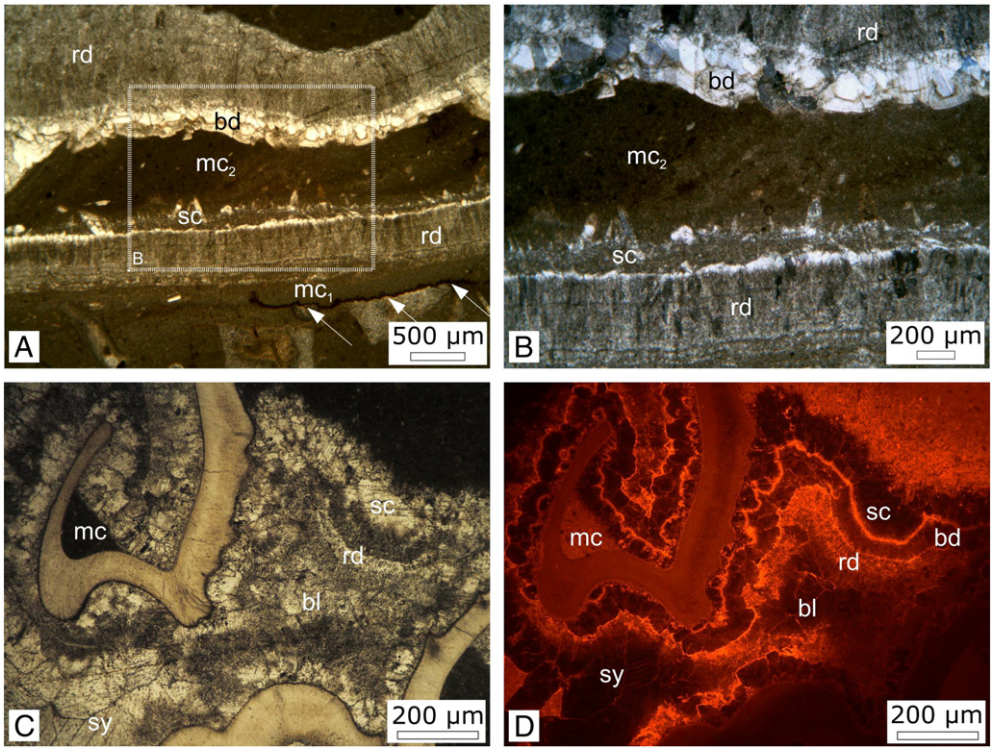

Fig. 7. Photomicrographs of Jebel el Oftal (JeO) mound carbonate rocks. A) Dyke fills paragenetic sequence showing trace of dissolution (arrows). Dykes in JeO mounds are filled with two generations of micrite (mc_1, mc_2), isopachous crusts of radiaxial fibrous calcite (rd), scalenohedral calcite (sc) and bladed calcite (bd). Plane polarized light. B) Close up of the dyke fill (box in A), cross-polarized light. C) Transmitted light photomicrograph of the trilobite-bearing floatstone (sample 33). Skeletal remains are partially filled by geopetal micrite (mc). D) Cathodoluminescence photomicrograph (same as C) showing cements paragenesis: scalenohedral calcite (sc), bladed calcite (bd); radiaxial fibrous calcite (rd); blocky calcite (bl); syntaxial calcite (sy).

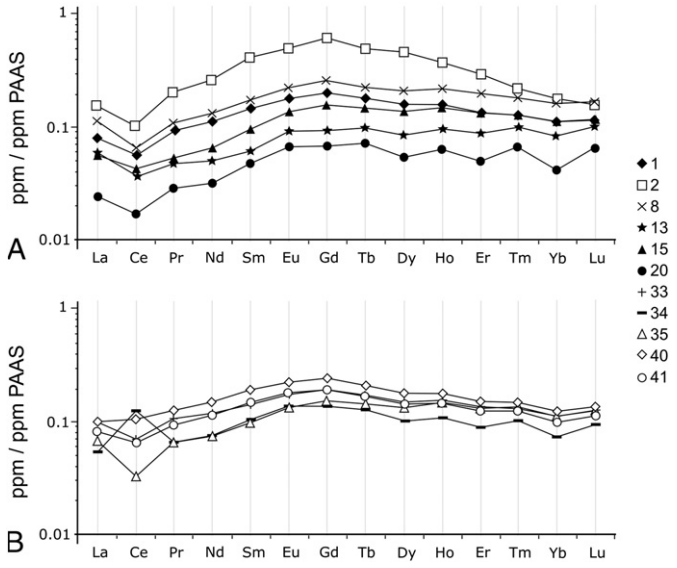

Fig. 8. PAAS-normalized REE patterns of GeM (A) and JeO (B) bulk samples.

sample (sample 2) are characterized by LREE fractionation, slight MREE enrichment, slightly negative Ce anomaly, lack of Gd anomaly and pos itive Eu anomaly. Dolomite from GeM (sample 2) shows high ΣREE con tent (33.5 ppm) bulged MREE pattern ($Tb_{SN}/Yb_{SN} = 2.84$) and high Gd anomaly.

Table 2 shows REE and selected trace element distribution from the carbonate sub samples. Th content ranges between 0.00 ppm and 0.82 ppm. Whereas the concentrations of Mo and U range from 0.00 to 0.09 ppm and from 0.01 to 0.25 ppm, respectively. REE patterns of carbonate sub samples are reported in Fig. 9. The REE pattern of micritic sub samples shows low LREE fractionation (average $Pr_{SN}/Yb_{SN} = 0.82$), and slightly bulged MREE pattern (average Tb_{SN}/Yb_{SN} up to 1.62). The layered micrite from dyke fills shows clear LREE fractionation, lower ΣREE, and negative Ce anomaly (Fig. 9A). Generally the micrite samples yielded the higher ΣREE values (between 4.9 ppm and 42.9 ppm; average 16.7 ppm), a chondritic Y/Ho ratio (average 47.6), a positive La anomaly ($1.05 < La^* < 1.66$), an overall positive Eu anomaly ($1.05 < Eu^* < 1.31$), a positive Gd anomaly ($0.99 < Gd^* < 1.24$), and a highly variable Ce anomaly (spanning from 0.50 to 2.37) (Table 2). Cement sub samples from mound facies and stromatactis like cavities (Fig. 9B) show a different REE pattern with strong LREE fractionation ($Pr_{SN}/Yb_{SN} = 0.57$). The ΣREE content of cements in all the sub sampled facies is lower than micrite with average values of 7.2 ppm and 4.7 ppm for mound facies and stromatactis like cavities, respective ly. Cement samples have super chondritic Y/Ho values (average 62.7), a positive La anomaly (average 1.41), an overall negative Ce anomaly (average 0.68), and slightly positive Eu and Gd anomalies (average 1.14 and 1.08, respectively). Hematite rich vein fills have a peculiar REE pattern (Fig. 9A) with very low ΣREE, as low as 1.2 ppm, a super-chondritic Y/Ho ratio (up to107.6), a strong LREE enrichment (average $Pr_{SN}/Yb_{SN} = 2.93$), a positive La, Eu and Gd anomaly (average 1.30, 1.31 and 1.34, respectively) and no Ce anomaly (Table 2).

6. Discussion

6.1. REE pattern of marine precipitates

The average shale normalized REE patterns are rather consistent throughout the carbonate dataset. Nevertheless, bulk samples from mound micrite, dykes and vein fills show different REE distribution (Fig. 8). Moreover, micritic sub sampled phases appear to have different REE trends with respect of sub sampled cements (Fig. 9). Carbonate precipitates in marine environment are thought to have a normal marine REE pattern typified by i) strong LREE depletion (e.g., Olivier and Boyet, 2006), ii) negative Ce and positive La anomalies and iii) pos itive Gd anomaly (between 1.1 and 1.3, de Baar et al., 1985; Zhang and Nozaki, 1998). The starting assumptions here are that i) non skeletal carbonates incorporate REE in equilibrium with seawater (Webb and Kamber, 2000), ii) seawater REE patterns have hardly changed through out the Phanerozoic (Shields and Webb, 2004), iii) HREE enrichment has been a characteristic feature of seawater since the late Archaean

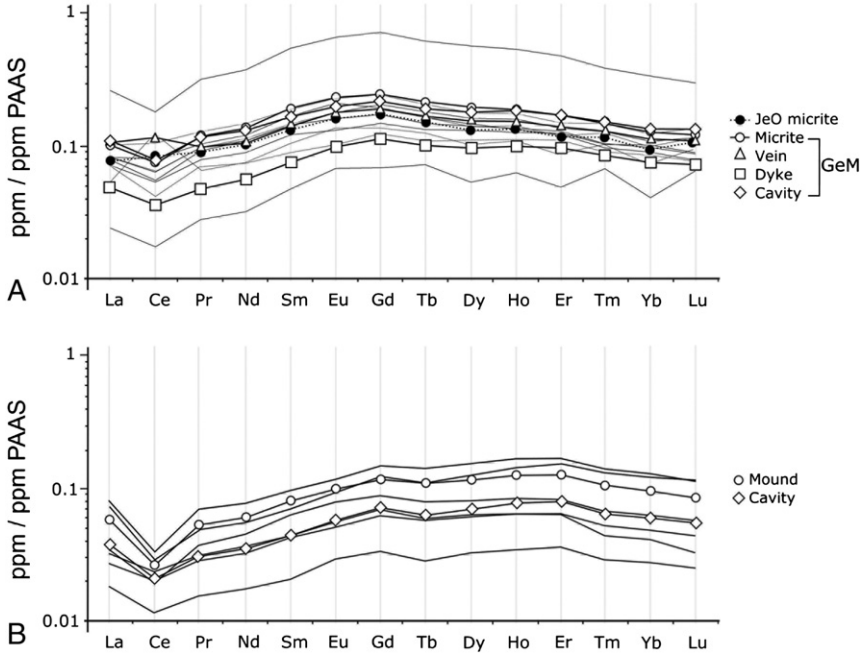

Fig. 9. PAAS-normalized REE patterns of GeM and JeO sub-samples. A) Mound micrite patterns (continuous black lines) and average patterns from GeM, JeO, vein, dykes and stromatactis-like cavities fills. B) Carbonate cements patterns and average patterns from mound and cavity fills.

(Bau and Dulski, 1996; Kamber and Webb, 2001; Shields and Webb, 2004), and iv) REE in carbonate tend to be relatively immobile during diagenesis (Banner et al., 1988; Webb and Kamber, 2000; Van Kranendonk et al., 2003; Bolhar et al., 2004; Kamber et al., 2004; Nothdurft et al., 2004; Webb et al., 2009; Della Porta et al., 2015). There fore, the mixing of seawater with other fluids, such as hydrothermal fluids, can have an effect on the chemistry of carbonate precipitates that may deviate from that of the normal seawater pattern (Michard, 1989; Klinkhammer et al., 1994; Douville et al., 1999). REE patterns of marine limestones could also be complicated by possible modification due to the presence of i) REE bearing terrigenous matter (Goldstein and Jacobsen, 1988; Elderfield et al., 1990), ii) phosphates, which have a high affinity for REE in diagenetic fluids and in some cases show non uniform incorporation (German and Elderfield, 1990; Byrne et al., 1996) and iii) Fe and Mn oxides, which incorporate REE disproportion ately (Bau et al., 1996; Bayon et al., 2004).

The analytical method used for the preparation of carbonate sub samples (see Rongemaille et al., 2011) should guarantee a good reliability of REE data from carbonate phases avoiding REE contribution from contaminants. Nevertheless, especially for the bulk samples, even a small amount of phosphates (e.g., German and Elderfield, 1990; Reynard et al., 1999) and/or terrigenous matter is able to mask the sea water signature. Within the bulk limestones, P contents show a negative correlation with ΣREE ($R = -0.75$ $P = 0.0039$), whilst Al and Rb, used as indicators of terrigenous contamination (e.g., Webb and Kamber, 2000; Nothdurft et al., 2004; Allwood et al., 2010), show a weak corre lation (lower statistical significance) with ΣREE ($R = 0.63$ $P = 0.0189$ and $R = 0.68$ $P = 0.0107$, respectively). Moreover, Fe contents show positive correlation with Pr_{SN}/Yb_{SN} in most of the bulk carbonates analysed suggesting that diagenetic Fe might have influenced REE pat terns mobilizing LREE in the carbonates lattice (e.g., Nothdurft et al., 2004). The [ΣREE/Fe] ratio of 0.015 ± 3 is consistent for all but three samples (Table 2). Kaufmann (1997) discussed the presence of Fe with in the carbonate fraction as diagenetic in origin. Mobilization of this Fe may have triggered disproportional REE incorporation from pore water resulting in an overall increase of ΣREE (and LREE).

Hence, whilst only bulk samples analyses might have been biased by the presence of terrigenous contaminants, most of the carbonates analysed show good correlation between Fe contents and either ΣREE or LREE enrichment.

6.2. MB carbonate paragenesis

The study of the MB carbonates needs to consider the variation of mineralogy and chemistry that likely occurred during the early diagenesis and the characteristic of the seawater. Since these carbonate phases may have formed over a range of physicochemical and diagenetic conditions, the exploration of the conditions associated with their formation requires that the carbonate paragenesis is properly constrained. The paragenesis of MB carbonates in fact, by retaining a zonation of the cements (Fig. 7), clearly reflects the pore water variation and fluctuation of chemical composition. The starting assumption is that parautochthonous bioclasts have been cemented by pristine micrite deposed in alkaline pore water probably triggered by microbial activity (e.g., Kaufmann, 1998a, 1998b). By assuming that the Devonian was a period dominated by calcite seas (e.g., Balthasar and Cusak, 2015), the high Mg calcite found as fibrous isopachous cement (Figs. 4A, 7) could be regarded as the likely product of early marine diagenesis (radiaxial calcite; Kaufmann, 1997). This marine calcite cement is locally followed by shallow burial, bright and banded luminescent cements (Fig. 7C D) reflecting high variability of pore water chemistry within a partially closed system (cf. Kaufmann, 1997). Likewise, after this shallow burial cement's formation, the diagenesis did not affect the REE distribution that will eventually reflect the pore water composition (Banner et al., 1988; Webb and Kamber, 2000; Van Kranendonk et al., 2003; Bolhar et al., 2004; Kamber et al., 2004; Nothdurft et al., 2004; Webb et al., 2009; Della Porta et al., 2015). Although it was sometimes impossible to separate radiaxial cements from blocky calcite and other burial phases (Table 2), the chemical data set presented here shows a rather consistent evidence of the difference between micrite and cements (considered as a whole) in terms of chemical composition.

An interesting aspect is represented by the paragenetic sequence that fills the neptunian dykes at JeO and shows evidence of dissolution of micrite and bioclasts within the lithified wackestone (Fig. 7A). The dissolution is followed by new generations of micrite and radiaxial isopachous calcite (Fig. 7A B). The dyke is then filled by micrite, probably allochthonous in origin, as suggested by the higher amount of terrig enous materials (Fig. 7B). This evidence of diagenetic reactivation, and presumable input of fluids and materials from higher strata (Fig. 3G), might have influenced the overall chemistry of carbonates and dykes that cross them, including some mobilization of REE from micrite to ce ment. The reactivation of the carbonate system during the dyke forma tion is corroborated by the peculiar REE pattern found in the dyke fills (Fig. 9A) that shows normal marine characteristics.

The MB mounds were affected by burial diagenesis as suggested by Fe enrichment (cf. Kaufmann, 1997) in burial cements (i.e. blocky and syntaxial calcite in Fig. 7C D). The presence of scattered dolomite crystals (Fig. 4B) within the mound micrite might be related either to the in cipient burial diagenesis or to circulation of mineralizing fluids; this latter event being probably related to the formation of the dolomitized wedge described at GeM (Fig. 4C D). This dolomitization process might suggest mobilization of REE at a later stage after the mound for mation. The finding that Lower Carboniferous carbonates which had undergone two separate phases of dolomitization retained their orig inal seawater REE patterns (Banner et al., 1988), however, suggested that, unless a complete dissolution of the minerals had taken place, REE can be considered as relatively stable within MB mound carbonates (Banner et al., 1988; Webb and Kamber, 2000; Van Kranendonk et al., 2003; Bolhar et al., 2004; Kamber et al., 2004; Nothdurft et al., 2004; Webb et al., 2009; Della Porta et al., 2015). Although some modification in the paragenesis may have occurred (i.e. corrosion of micrite and blad ed calcite in the dyke system, Fig. 7), the cathodoluminescence analyses seem to exclude a total dissolution of carbonate minerals. Whether a uniform cathodoluminescence may be evidence of diagenetic overprint, a wide variation in luminescence suggests variation of Fe/Mn within pore water and, therefore, it can be an evidence of the preservation of the original carbonate paragenesis (Sommer, 1972). Assuming a relative overall stability of REE within the carbonate lattice during diagenesis, the diverse carbonate facies that were formed under different physico chemical conditions and from different fluids mixing should, therefore, yield different original REE patterns. Indeed, the analyses carried out on bulk samples from different facies showed variable geochemical composition of the carbonates. Moreover, both micrite and cement (Tables 1 2) revealed an overall different REE trends (Fig. 9). Micrite ap pears enriched in ΣREE if compared with other cements that exhibit a clear marine pattern: low ΣREE, super chondritic Y/Ho ratio (up to 75.9), LREE fractionation (average $Pr_{SN}/Yb_{SN} = 0.58$) and a slightly positive Gd anomaly (Table 2). Mound micrite exhibits a bulged REE pattern (average $Tb_{SN}/Yb_{SN} = 1.65$) and an anomalously high Ce anomaly (Table 2) revealing the likely precipitation from oxic to suboxic pore water (Haley et al., 2004). A similar REE enrichment within micrite has also been described from the Kess Kess mud mounds and considered to be the result of the combined effect of kinetics and microbial induced enrichment (see discussion in Franchi et al., 2015). By comparing bulk sample (white in Table 2) analyses with results from micrite and cement sub samples (grey in Table 2), it was possible to assess which particular carbonate phases were dominant in the defi nition of bulk sample REE pattern (Fig. 10). Bulk sample composition of sample 8 for instance reflects a micrite REE pattern showing MREE bulged pattern and high ΣREE contents whereas the cement phase has a marine like pattern (Fig. 10A). Similar overlap of bulk sample and micrite patterns is yielded by sample 33 (Fig. 10B) where cement

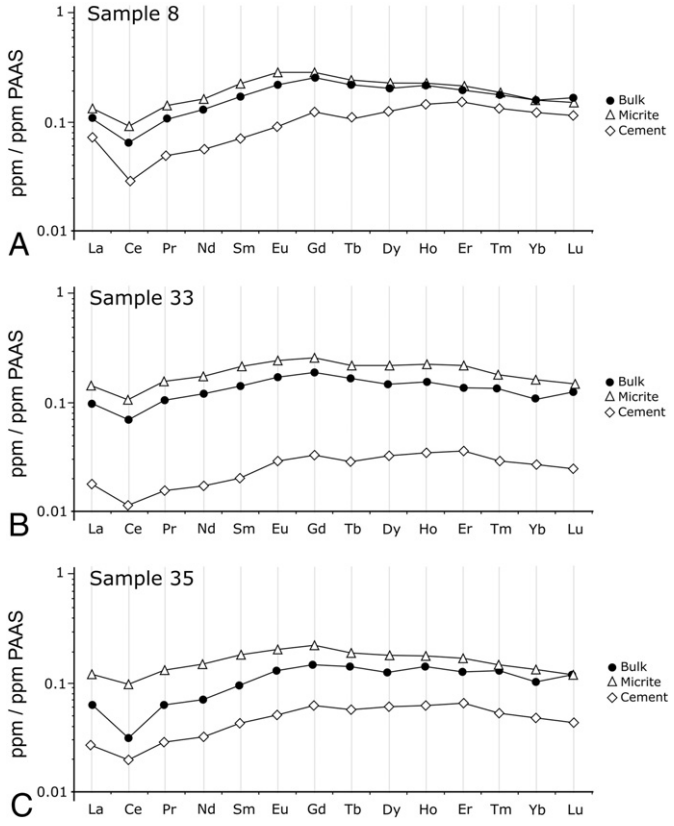

Fig. 10. Comparison of bulk specimen, micrite and cement PAAS-normalized REE patterns of selected samples: A) sample 8. B) sample 33. C) sample 35.

ΣREE is one order of magnitude lower than micrite. By contrast sample 35 shows a consistent shift of bulk rock pattern from micrite pattern (Fig. 10C).

6.3. Mineralizing fluids and palaeoredox conditions

Part of the diagenetic history of GeM mound can be unravelled by tracking the nature of fluids circulating through the sediments during mound early diagenesis and the variation of the redox conditions within pore water.

Mo can be used as a tracer for anoxic conditions (e.g., Neubert et al., 2008). In well oxygenated water Mo shows a conservative behaviour being present as molybdate (MoO_4^{2-}), whilst it is normally enriched, as thiomolybdate (MoS_4^{2-}), within organic matter and iron sulphides under anoxic conditions (Helz et al., 1996; Neubert et al., 2008; Algeo and Tribovillard, 2009). In such conditions, Mo is completely removed from seawater and accumulated in surface sediments (Neubert et al., 2008). The rate of Mo scavenging from seawater depends on the dissolved sulphide concentration (Neubert et al., 2008 and references therein). In MB carbonates, the Mo contents (average 0.05 ppm) appear far below the crustal average of 1 2 ppm (Taylor and McLennan, 1985), and close to the pure carbonates concentration of 0.02 ppm (Neubert et al., 2008). Carbonates are the main Mo bearing phases of the studied samples since Mo in the residuum is below the detection limit (Supplementary materials S1). As shown in Table 3, the highest Mo_{EF} (and U_{EF}) values were found from samples with lower Al_2O_3 contents (Supplementary material S1), and extremely low Al_2O_3 may even lead to high and unrealistic EF. Samples with high Mo_{EF} (and U_{EF}) values also show the lower ΣREE contents (Table 3 and Supplementary mate rial S1). Apart from these samples, we found that Mo is particularly enriched in the carbonates from mound facies (Table 3). Low values of Mo_{EF}/U_{EF} are probably due to the increasing uptake of U onto the authigenic fraction (Algeo and Tribovillard, 2009) under more reducing conditions (sub oxic) within the Fe reduction zone (Hu et al., 2014). Such conditions were likely to occur during precipitation of vein fills and, in particular, during the formation of dolomitized limestones (sample 2) at GeM (Table 3). Although the overall low concentrations of Mo, U and Al_2O_3 may produce a bias for EF calculation, we may infer that these variable Mo_{EF}/U_{EF} ratios are probably due to vari able redox conditions (Hu et al., 2014) reflecting difference in pore water fluid composition, alkalinity and sulphate concentrations be tween mineralizing fluids which precipitated mound micrite, dyke and vein fills.

Studies of REE distributions in modern and ancient carbonates re - vealed that the partition of Eu and Ce during the formation of authigenic carbonates can be related to redox conditions (e.g., Pourret et al., 2008; Hu et al., 2014). Eu is particularly enriched in high temperature hydro thermal fluids emanating from oceanic crust due to plagioclase break down resulting in a strong positive Eu anomaly (e.g., Douville et al., 1999; Klinkhammer et al., 1994). Eu, which is present as Eu(III) in sea water, is reduced to the strongly mobile Eu(II) within the interstitial fluids under reducing conditions (MacRae et al., 1992; Guy et al., 1999; Martinez Ruiz et al., 1999) giving rise to a strongly positive Eu anomaly. The highest values of Eu shown in the studied samples come from the hematite rich micrite that fills the veins (Table 2). The overall ΣREE depletion, LREE enrichment, and strong Eu anomaly of the vein fill hematite rich micrite suggest a relationship with hydrothermal fluids (e.g., Bau and Dulski, 1999).

Among lanthanides, Ce is the only one that can be oxidized to (IV) and may help in assessing the redox conditions during carbonate precipitation. In general, carbonates precipitated from well oxygenated seawater retain a consistent negative Ce anomaly, whilst a high positive Ce anomaly is found in those carbonates deposited under poorly oxygenated conditions (e.g., Haley et al., 2004; Olivier and Boyet, 2006; Oliveri et al., 2010). Under oxic conditions, Ce(III) is rapidly oxidized to insoluble Ce(VI) ions, which can be easily scavenged by Fe oxyhydroxides (e.g., Derry and Jacobsen, 1990) and organic matter (e.g., Kim et al., 2012; Hu et al., 2014). Therefore, a Ce anomaly below 0.5 suggests oxygenated oceanic conditions (e.g., Haley et al., 2004), whereas a positive Ce anomaly might be in duced by anoxic conditions (Olivier and Boyet, 2006; Oliveri et al., 2010; Hu et al., 2014) and/or diagenetic decomposition of Ce bearing organic matter (e.g., Pourret et al., 2008). It has been demon strated that oxidation of Ce(III) to Ce(IV) can be induced by bacterial mediation (e.g., Moffett, 1994) or abiotically through Fe Mn oxyhydroxide activity (e.g., Bau, 1999). Pourret et al. (2008) demon strated that pH plays a major role in REE complexation and an in crease of pH may induce a consistent Ce anomaly. The presence of dispersed organic matter (DOC) may inhibit the development of Ce anomaly through competition between DOC and carbonates for the complexation of REE (Dia et al., 2000; Davranche et al., 2005). At high car bonate alkalinity and a pH over 8.0, Ce(IV) can be adsorbed by organic matter leading to a positive Ce anomaly of the organic rich colloids and consequent negative Ce anomaly of the solution (Pourret et al., 2008; Himmler et al., 2010; Kim et al., 2012; Hu et al., 2014). In such conditions, typical of highly reducing pore water fluids at methane seeps (Himmler et al., 2010), the Ce anomaly in the carbonates can be disguised (Ce^* ~1). The average Ce anomaly yielded by GeM mound micrite (0.75) and dike fill (0.85) samples may therefore suggest a precipitation of micrite controlled by high pH and alkalinity under oxic to suboxic conditions within organic rich sediments. Dissolution/remineralization of or ganic matter during the early diagenesis may lead to the release of Ce (IV) within the inorganic precipitates (i.e. carbonates) that normally would yield a normal marine negative Ce anomaly.

Whether or not GeM mound micrite and dyke fills reflect precipitation from variable oxygenated marine water, veins have been probably affected by circulation of poorly oxygenated (average $Ce^* = 1.22$) Fe bearing fluids.

6.4. Microbial activity

Trace element and REE distribution within GeM carbonates appears to be consistent with precipitation in alkaline, organic matter rich pore water. The bulk of the fine grained carbonates of the MB mounds was described as microbial boundstone (Kaufmann, 1996, 1997) locally retaining traces of photoautotrophs (e.g., cyanobacteria in Kaufmann, 1998a). The authigenic micrite may have precipitated within the extra cellular polymeric substances (EPS) generated by microbial communi ties that are regarded to have flourished below the base of storm waves in an euphotic environment (Kaufmann, 1996, 1998a), where the physicochemical properties of the water would have allowed the microbial communities to fix $CaCO_3$ in their biofilms (e.g., Chafetz and Buczynski, 1992; Monty, 1995). This assumption, however, apparently contradicts earlier paleoenvironmental reconstructions that placed the MB mounds well below the euphotic zone in deep and cold water (Wendt, 1993; Kaufmann, 1995, 1997). Nevertheless, the eye catching final results are the steep flanks of the carbonates mounds.

Despite the rarity of direct evidences of microbial activity, potential microbial derived features, such as peloidal micrite and amalgamated clots, can be said to exist especially within the carbonate filling of dykes and veins (Fig. 4E G) and as microbial boundstone (Kaufmann, 1996, 1997) or calcimicrobes associated to stromatactis cavities (Kaufmann, 1998a). Because of the cause effect relationships between microbial activity, micro environment, and changes of REE behaviour, the ability of microbial communities to fix higher amounts of REE within the sediments through their EPS (e.g., Webb and Kamber, 2000; Nothdurft et al., 2004) should be carefully considered. Accordingly, high REE contents within mound micrite with respect to early and burial diagenetic cements (Figs. 9, 10) may be related to an increase of alkalinity due to microbial consumption of the abundant organic matter within the sediments provided by the flourishing benthic fauna (i.e. crinoids; Kaufmann, 1997). Further evidence of this effect might be the overall high Ce^*/Ce values from GeM micrites ($0.66 < Ce^*/Ce < 0.89$) and dyke fills ($0.79 < Ce^*/Ce < 0.96$). As discussed above, the microbial degradation of organic matter may release high amounts of REE, oxidize Ce (Moffett, 1994) and disguise the seawater REE pattern (e.g., Kim et al., 2012).

Therefore, ruling out the consequences of terrigenous contamination (see Section 6.1), the likely source of REE enrichment within MB car bonates might be due to microbial activity or to kinetic factors (Franchi et al., 2015; Jakubowicz et al., 2015a) and/or incorporation of allochthonous micrite.

7. Concluding remarks

The MB conical mounds have steep flanks and a pure carbonate composition dominated by calcite. Bulk of the mounds consists of stromatactis bearing wackestone, grainstone and floatstone. GeM mound is cross cutted by systems of neptunian dykes and veins. Several considerations can be drawn considering dyke and vein fills as well as REE distributions in the different carbonate phases from GeM mound.

1. In the neptunian dykes, mixed Givetian brachiopod fauna may also include younger taxa as suggested by the presence of the atrypids *Desquamatia sp.* and *C. marocanensis* within the limestone pebbles engulfed in the dyke infill. The dykes allowed fluid injection within the system as well as the corrosion of micrite and bioclasts that may have induced a diagenetic modification of the paragenesis, in cluding some mobilization of REE. REE patterns of the dyke fills reflect a precipitation of carbonates under normal marine conditions. Presence of peloidal micrite and the Ce anomaly values close to 1 may suggest a strong microbial activity during precipitation of dyke fills micrite.
2. Whether or not the chemistry of neptunian dyke fills recorded normal marine conditions, the precipitation of hematite rich carbonates within the vein systems of the GeM mound has probably been trig gered by activity of microbial consortia and the circulation of anoxic fluids. Evidences of the microbial activity are the peloidal and clotted fabrics preserved within the carbonate filling the veins. Vein fills show bulge REE pattern typical of carbonates deposed within Fe(III) Fe(II) transition zone in sub oxic conditions. Also, the vein fills show an overall depletion in □REE if compared with other car bonate facies, high Eu anomaly and LREE enrichment suggesting a likely mixing with hydrothermal water (cf. Bau and Dulski, 1999).
3. The REE pattern of the GeM mound micrite is characterized by frac tionated LREE, positive Gd anomaly and overall MREE enrichment resulting in a slightly bulged pattern. High REE contents coupled with the lack of a Ce anomaly and low Mo contents point toward a micrite formation within high alkaline, oxygenated pore water with high organic matter contents rather than seawater mixing with poorly oxygenated fluids (i.e. hydrothermal fluids). The microbial degradation of organic matter during early diagenesis into high alkaline pore water may result in the overall REE enrichment and disguise the seawater REE pattern of the MB carbonates. Initially, the organic compounds scavenge the dissolved Ce(IV) displaying a strong positive Ce anomaly (coupled with HREE enrichment) with a concomi tant negative Ce anomaly in the pore fluids. Then, during early diagenesis, consumption of organic matter mediated by a microbial consortium increases pore water alkalinity triggering the precipita tion of authigenic carbonates with Ce anomaly close to 1.
4. In conclusion we may consider mound micrite as characteristic of the conditions during the early diagenesis of the mound buildup with high alkalinity, high pH, and presumably high organic matter con tents resulting in overall ΣREE enrichment, whilst hematitized carbonates as characteristic of late fluid circulation characterized by super chondritic Y/Ho ratio and very low ΣREE content. The study of REE distribution within different carbonate phases does not address crucial questions such as the depth of formation of MB mounds. Nevertheless the geochemical characterization of micrite and cement from GeM suggests a precipitation of these phases under oxic to suboxic conditions. In this scenario, the venting fluids had a marginal role in the early lithification of the MB mounds. The process of lithification of the steep flanks of the mounds has been rather favoured by high pore water alkalinity and probably fostered by microbial metabolic reaction linked to elevated organic matter contents.

Supplementary data to this article can be found online at http://dx.doi.org/10.1016/j.sedgeo.2016.07.008.

Acknowledgements

This research was supported by the MIUR grant (PRIN 2010) to R. Barbieri. We are indebted with one of the reviewer, Christian Klug, for his precious comments on the first version of this manuscript, and to Frances Keenan for her thorough English revision. The authors would like to thanks L. Martire (University of Turin) and C. Mazzoli (University of Padua) for the precious advices and access to facilities for CL analyses. We thank A. Hofmann (University of Johannesburg) for constructive comments on the topic of this paper. Thanks are due to C. Reinke and E. Fisher (University of Johannesburg) for their techni cal assistance and to S. Sathiaraj (BIUST) for the access to XRD facilities.

References

Algeo, T., Tribovillard, N., 2009. Environmental analysis of paleoceanographic systems based on molybdenum–uranium covariation. Chemical Geology 268, 211–225. Allwood, A.C., Kamber, B.S., Walter, M.R., Burch, I.W., Kanik, I., 2010. Trace elements record depositional history of an Early Archean stromatolitic carbonate platform. Chemical Geology 270, 148–163.

Aretz, M., Herbig, H.-G., 2010. Corals from the Viséan of the central and southern part of Azrou-Khénifra Basin (Carboniferous, Central Moroccan Meseta). Palaeoworld 19, 294–305.

Baidder, L., Michard, A., Soulaimani, A., Fekkak, A., Eddebbi, A., Rjimati, E.-C., Raddi, Y., 2016. Fold interference pattern in thick-skinned tectonics; a case study from the

External Variscan Belt of Eastern Anti-Atlas, Morocco. Journal of African Earth Sciences. http://dx.doi.org/10.1016/j.jafrearsci.2016.04.003.
Balthasar, U., Cusak, M., 2015. Aragonite-calcite seas—quantifying the gray area. Geology 43, 99–102.
Banner, J.L., Hanson, G.N., Meyers, W.J., 1988. Rare earth element and Nd isotopic variations in regionally extensive dolomites from the Burlington-Keokuk Formation (Mississippian): implications for REE mobility during carbonate diagenesis. Journal of Sedimentary Petrology 58, 415–432.
Bau, M., 1999. Scavenging of dissolved yttrium and rare earths by precipitating iron oxyhydroxide: experimental evidence for Ce oxidation, Y–Ho fractionation, and lan-thanide tetrad effect. Geochimica et Cosmochimica Acta 63, 67–77.
Bau, M., Dulski, P., 1996. Distribution of yttrium and rare-earth elements in the Penge and Kuruman iron-formations, Transvaal Supergroup, South Africa. Precambrian Research 79, 37–55.
Bau, M., Dulski, P., 1999. Comparing yttrium and rare earths in hydrothermal fluids from the Mid-Atlantic Ridge: implications for Y and REE behaviour during near-vent mixing and for the Y/Ho ratio of Proterozoic seawater. Chemical Geology 155, 77–90. Bau, M., Koschinsky, A., Dulski, P., Hein, J.R., 1996. Comparison of the partitioning behav-iours of yttrium, rare earth elements, and titanium between hydrogenetic marine ferromanganese crusts and seawater. Geochimica et Cosmochimica Acta 60, 1709–1725.
Bayon, G., German, C.R., Burton, K.W., Nesbitt, R.W., Rogers, N., 2004. Sedimentary Fe–Mn oxyhydroxides as paleoceanographic archives and the role of aeolian flux in regulat-ing oceanic dissolved REE. Earth and Planetary Science Letters 224, 477–492.
Bełka, Z., 1998. Early Devonian Kess-Kess carbonate mud mounds of the eastern Anti-Atlas (Morocco), and their relation to submarine hydrothermal venting. Journal of Sedimentary Research 68, 368–377.
Bełka, Z., Berkowski, B., 2005. Discovery of thermophilic corals in an ancient hydrothermal vent community, Devonian, Morocco. Acta Geologica Polonica 55, 1–7.
Biernat, G., Szulczewski, M., 1975. The Devonian brachiopod *Phlogoiderhynchus polonicus* (Roemer, 1866) from the Holy Cross mountains, Poland. Acta Palaeontologica Polonica 20, 199–229.
Bolhar, R., Kamber, B.S., Moorbath, S., Fedo, C.M., Whitehouse, M.J., 2004. Characterisation of early Archaean chemical sediments by trace element signatures. Earth and Planetary Science Letters 222, 43–60.
Brachert, T.C., Buggisch, W., Flügel, E., Hüssner, H.M., Joachimski, M.M., Tourneur, F., Walliser, O.H., 1992. Controls of mud mound formation: the Early Devonian Kess-Kess carbonates of the Hamar Laghdad, Antiatlas, Morocco. Geologische Rundschau 81, 11–44.
Burkhard, M., Caritg, S., Helg, U., Robert-Charrue, C., Soulaimani, A., 2006. Tectonics of the Anti-Atlas of Morocco. Comptes Rendus Geoscience 338, 11–24.
Byrne, R.H., Liu, X., Schijf, J., 1996. The influence of phosphate coprecipitation on rare earth element distributions in natural waters. Geochimica et Cosmochimica Acta 60, 3341–3346.
Cavalazzi, B., 2007. Chemotrophic filamentous microfossils from the Hollard Mound (Devonian, Morocco) as investigated by focused ion beam. Astrobiology 7, 402–415.
Cavalazzi, B., Barbieri, R., Ori, G.G., 2007. Chemosynthetic microbialites in the Devonian carbonate mounds of Hamar Laghdad (Anti-Atlas, Morocco). Sedimentary Geology 200, 73–88.
Cavalazzi, B., Barbieri, R., Cady, S.L., George, A.D., Gennaro, S., Lui, A., Westall, F., Rossi, A.P., Ori, G.G., Taj-Heddine, K., 2012. Iron-framboids in the hydrocarbon-related Middle Devonian Hollard Mound of the Anti-Atlas mountain range in Morocco: evidence of potential microbial biosignatures. Sedimentary Geology 263-264, 183–193.
Chafetz, H.S., Buczynski, C., 1992. Bacterially induced lithification of microbial mats. PALAIOS 7, 277–293.
Chafiki, D., Canérot, J., Souhel, A., El Hariri, K., Taj Eddine, K., 2004. The Sinemurian carbonate mud-mounds from central High Atlas (Morocco): stratigraphy, geometry, sedimentology and geodynamic patterns. Journal of African Earth Sciences 39, 337–346.
Della Porta, G., Webb, G.E., McDonald, I., 2015. REE patterns of microbial carbonate and cements from Sinemurian (Lower Jurassic) siliceous sponge mounds (Djebel Bou Dahar, High Atlas, Morocco). Chemical Geology 400, 65–86.
De Baar, H.J.W., Bacon, M.P., Brewer, P.G., Bruland, K.W., 1985. Rare earth elements in the Pacific and Atlantic oceans. Geochimica et Cosmochimica Acta 49, 1943–1959.
De Mol, B., Henriet, J.-P., Canals, M., 2005. Development of coral banks in Porcupine Seabight: do they have Mediterranean ancestors? In: Freiwald, A., Roberts, J.M. (Eds.), Cold-Water Corals and Ecosystems. Springer, Berlin Heidelberg, pp. 515–533 De Mol, L., Van Rooij, D., Pirlet, H., Greinert, J., Frank, N., Quemmerais, F., Henriet, J.-P., 2011. Cold-water coral habitats in the Penmarc'h and Guilvinec canyons (Bay of Biscay): deep-water versus shallow-water settings. Marine Geology 282, 40–52.
Derry, L.A., Jacobsen, S.B., 1990. The chemical evolution of Precambrian seawater: evidence from REEs in banded iron formations. Geochimica et Cosmochimica Acta 54 2965-1977.
Davranche, M., Pourret, O., Gruau, G., Dia, A., Le Coz-Bouhnik, M., 2005. Adsorption of REE(III)–humate complexes onto MnO_2: experimental evidence for cerium anomaly and lanthanide tetrad effect suppression. Geochimica et Cosmochimica Acta 69, 4825–4835.
Dia, A., Gruau, G., Olivié-Lauquet, G., Riou, C., Molénat, J., Curmi, P., 2000. The distribution of rare earth elements in groundwaters: assessing the role of sourcerock composition, redox changes and colloidal particle. Geochimica et Cosmochimica Acta 64, 4131–4151.
Döring, S., Kazmierczak, M., 2001. Stratigraphy, geometry, and facies of a Middle Devonian ramp-to-basin transect (Eastern Anti-Atlas, SE Morocco). Facies 44, 137–150.
Douville, E., Bienvenu, P., Charlou, J.L., Donval, J., Fouquet, Y., Appriou, P., Gamo, T., 1999Yttrium and rare earth elements in fluids from various deep-sea hydrothermal systems. Geochimica et Cosmochimica Acta 63, 627–643.
Dumestre, A., Illing, L.V., 1967. Middle Devonian reefs in Spanish Sahara. In: Oswald, D.H. (Ed.), International Symposium on the Devonian System. J. Alberta Soc. Petrol. Geol Vol. 2, pp. 333–350.
Elderfield, H., Upstill-Goddard, R., Sholkovitz, E.R., 1990. The rare earth elements in rivers, estuaries and coastal sea waters: processes affecting crustal input of elements to the ocean and their significance to the composition of sea water. Geochimica et Cosmochimica Acta 54, 971–991.
Feng, D., Chen, D., Peckmann, J., 2009. Rare earth elements in seep carbonates as tracers of variable redox conditions at ancient hydrocarbon seeps. Terra Nova 21, 49–56. Foubert, A., Henriet, J.-P., 2009. Nature and Significance of the Recent Carbonate Mound Record. Lecture Notes in Earth Sciences, 126. Springer-Verlag, Berlin, Heidelberg, p. 298.
Franchi, F., Schemm-Gregory, M., Klug, C., 2012. A new species of *Ivdelinia* Andronov, 1961 from the Moroccan Givetian and its palaeoecological and palaeobiogeographical implications. Bulletin of Geosciences 87, 1–11.
Franchi, F., Cavalazzi, B., Pierre, C., Barbieri, R., 2014. New evidences of hydrothermal fluids circulation at the Devonian Kess Kess mounds, Hamar Laghdad (eastern Anti-Atlas, Morocco). Geological Journal 50, 634–650.
Franchi, F., Hofmann, A., Cavalazzi, B., Wilson, A., Barbieri, R., 2015. Differentiating marine vs hydrothermal processes in Devonian carbonate mounds using rare earth elements (Kess Kess mounds, Anti-Atlas, Morocco). Chemical Geology 409, 69–86.
German, C.R., Elderfield, H., 1990. Application of the Ce anomaly as a paleoredox indicator: the ground rules. Paleoceanography 5, 823–833.
Goldstein, S.J., Jacobsen, S.B., 1988. Rare earth elements in river waters. Earth and Planetary Science Letters 89, 35–47.
Guy, C., Daux, V., Schott, J., 1999. Behaviour of rare earth elements during seawater/basalt interactions in the Mururoa Massif. Chemical Geology 158, 21–35.
Haley, B.A., Klinkhammer, G.P., McManus, J., 2004. Rare earth elements in pore waters of marine sediments. Geochimica et Cosmochimica Acta 68, 1265–1279.
Hebbeln, D., Samankassou, E., 2015. Where did ancient carbonate mounds grow—in bathyal depths or in shallow shelf waters? Earth Science Reviews 145, 56–65.
Helz, G.R., Miller, C.V., Charnock, J.M., Mosselmans, J.F.W., Pattrick, R.A.D., Garner, C.D., Vaughan, D.J., 1996. Mechanism of molybdenum removal from the sea and its concentration in black shales: EXAFS evidence. Geochimica et Cosmochimica Acta 60, 3631–3642.
Henriet, J.P., Hamoumi, N., Da Silva, A.C., Foubert, A., Lauridsen, B.W., Rüggeberg, A., Van Rooij, D., 2014. Carbonate mounds: from paradox to World Heritage. Marine Geology 352, 89–110.
Himmler, T., Bach, W., Bohrmann, G., Peckmann, J., 2010. Rare earth elements in authigenic methane-seep carbonates as tracers for fluid composition during early diagenesis. Chemical Geology 277, 126–136.
Hollard, H., 1974. Recherches sur la stratigraphie des formations du Dévonien moyen, de l'Emsien supérieur au Frasnien, dans le Sud du Tafilalt et dans le Maïder (Anti-Atlas oriental). Notes du Service Géologique du Maroc 264, 7–68.
Hu, Y., Feng, D., Peckmann, J., Roberts, H.H., Chen, D., 2014. New insights into cerium anomalies and mechanisms of trace metal enrichment in authigenic carbonate from hydrocarbon seeps. Chemical Geology 381, 55–66.
Jakubowicz, M., Dopieralska, J., Bełka, Z., 2015a. Tracing the composition and origin of fluids at an ancient hydrocarbon seep (Hollard Mound, Middle Devonian, Morocco): a Nd, REE and stable isotope study. Geochimica et Cosmochimica Acta 156, 50–74.
Jakubowicz, M., Berkowski, B., López Correa, M., Jarochowska, E., Joachimski, M., Bełka, Z., 2015b. Stable isotope signatures of Middle Palaeozoic Ahermatypic Rugose Corals – deciphering secondary alteration, vital fractionation effects, and palaeoecological implications. PloS One 10, e0136289. http://dx.doi.org/10.1371/journal.pone.0136289.
Johannesson, K.H., Hawkins Jr., D.L., Cortés, A., 2006. Do Archean chemical sediments record ancient seawater rare earth element patterns? Geochimica et Cosmochimica Acta 70, 871–890.
Kamber, B.S., Webb, G.E., 2001. The geochemistry of Late Archaean microbial carbonate: implications for ocean chemistry and continental erosion history. Geochimica et Cosmochimica Acta 65, 2509–2525.
Kamber, B.S., Bolhar, R., Webb, G.E., 2004. Geochemistry of late Archaean stromatolites from Zimbabwe; evidence for microbial life in restricted epicontinental seas. Precam-brian Research 132, 379–399.
Kaufmann, B., 1995. Middle Devonian mud mounds of the Ma'der Basin in the eastern Anti-Atlas, Morocco. In: Flajs, G., Vigener, M., Keupp, H., Meischner, D., Neuweiler, F., Paul, J., Reitner, J., Warnke, K., Weller, H., Dingle, P., Hensen, C., Schäfer, P., Gautret, P., Leinfelder, R.R., Hüssner, H., Kaufmann, B. (Eds.), Mud Mounds: A Polygenetic Spectrum of Fine-grained Carbonate Buildups. Facies Vol. 32, pp. 49–57.
Kaufmann, B., 1996. Facies, Stratigraphy and Diagenesis of Middle Devonian Reef and Mud-mounds in the Maïder (Eastern Anti-Atlas, Morocco) PhD thesis University of Tübingen.
Kaufmann, B., 1997. Diagenesis of Middle Devonian carbonate mud buildups of the Maïder Basin (eastern Anti-Atlas). Journal of Sedimentary Research A67, 945–956.
Kaufmann, B., 1998a. Middle Devonian reef and mud mounds on a carbonate ramp: Maïder Basin (eastern Anti-Atlas, Morocco). In: Wright, V.P., Burchette, T.P. (Eds.), Carbonate Ramps. Geol. Soc. Spec. Publ Vol. 149, pp. 417–435.
Kaufmann, B., 1998b. Facies, stratigraphy and diagenesis of Middle Devonian reef- and mud-mounds in the Maïder (eastern Anti-Atlas, Morocco). Acta Geologica Polonica 48, 43–106.
Kim, J.-H., Torres, M.E., Haley, B.A., Kastner, M., Pohlman, J.W., Riedel, M., Lee, Y.-J., 2012. The effect of diagenesis and fluidmigration on rare earth element distribution in pore fluids of the northern Cascadia accretionary margin. Chemical Geology 291, 152–165.
Klinkhammer, G.P., Elderfield, H., Edmond, J.M., Mitra, A., 1994. Geochemical implications of rare earth element patterns in hydrothermal fluids from mid-ocean ridges. Geochimica et Cosmochimica Acta 58, 5105–5113.

Lawrence, M.G., Greig, A., Collerson, K.D., Kamber, B.S., 2006. Rare earth element and yttrium variability in South East Queensland waterways. Aquatic Geochemistry 12, 39–72.
MacRae, N.D., Nesbitt, H.W., Kronberg, B.I., 1992. Development of a positive Eu anomaly during diagenesis. Earth and Planetary Science Letters 109, 585–591.
Martinez-Ruiz, F., Ortega-Huertas, M., Palomo, I., 1999. Positive Eu anomaly development during diagenesis of the K/T boundary ejecta layer in the Agost section (SE Spain): implications for trace-element remobilization. Terra Nova 11, 290–296. McLennan, S.M., 2001. Relationships between the trace element composition of sedimentary rocks and upper continental crust. Geochemistry, Geophysics, Geosystems 2 2000GC000109.
Michard, A., 1976. Elements de Géologie Marocaine. Notes et Mémoires du Service Géologique du Maroc 252, 1–408.
Michard, A., 1989. Rare earth element systematics in hydrothermal fluids. Geochimica et Cosmochimica Acta 53, 745–750.
Moffett, J.W., 1994. A radiotracer study of cerium and manganese uptake onto suspended particle in Chesapeake Bay. Geochimica et Cosmochimica Acta 58, 695–703.
Monty, C.L.V., 1995. The rise and nature of carbonate mud-mounds: an introductory actualistic approach. In: Monty, C.L.V., Bosence, D.W.J., Bridges, P.H., Pratt, B.R. (Eds.), Carbonate Mud-mounds: Their Origin and Evolution. Int. As. Sed Vol. 23, pp. 11–48.
Monty, C.L.V., Bosence, D.W.J., Bridges, P.H., Pratt, B.R., 1995. Carbonate mud-mounds. Their origin and evolution. International Association of Sedimentologists Special Pub-lication 23, p. 237.
Mounji, D., Bourque, P.A., Savard, M.M., 1998. Hydrothermal origin of Devonian conical mounds (Kess-Kess) of Hamar Laghdad Ridge, Anti-Atlas, Morocco. Geology 26, 1123–1126.
Neubert, N., Nagler, T.F., Böettcher, M.E., 2008. Sulfidity controls molybdenum isotope fractionation into euxinic sediments: evidence from the modern Black Sea. Geology 36, 775–778.
Nothdurft, L.D., Webb, G.E., Kamber, B.S., 2004. Rare earth element geochemistry of Late-Devonian reefal carbonates, Canning Basin, western Australia: confirmation of a sea-water REE proxy in ancient limestones. Geochimica et Cosmochimica Acta 68, 263–283.
Olivier, N., Boyet, M., 2006. Rare earth and trace elements of microbialites in Upper Jurassic coral- and sponge-microbialite reefs. Chemical Geology 230, 105–123.
Oliveri, E., Neri, R., Bellanca, A., Riding, R., 2010. Carbonate stromatolites from a Messinian hypersaline setting in the Caltanissetta Basin, Sicily: petrographic evidence of micro-bial activity and related stable isotope and rare earth element signatures. Sedimentol-ogy 57, 142–161.
Peckmann, J., Walliser, O.H., Riegel, W., Reitner, J., 1999. Signatures of hydrocarbon venting in a Middle Devonian carbonate mound (Hollard Mound) at the Hamar Laghdad (Antiatlas Morocco). Facies 40, 281–296.
Peckmann, J., Little, C.T.S., Gill, F., Reitner, J., 2005. Worm tube fossils from the Hollard Mound hydrocarbon-seep deposit, Middle Devonian, Morocco: Palaeozoic seeprelated vestimentiferans? Palaeogeography Palaeoclimatology Palaeoecology 227, 242–257.
Piqué, A., Michard, A., 1989. Moroccan Hercynides: a synopsis. The Paleozoic sedimentary and tectonic evolution at the northern margin of west Africa. American Journal of Science 289, 286–330.
Pourret, O., Davranche, M., Gruau, G., Dia, A., 2008. New insights into cerium anomalies in organic-rich alkaline waters. Chemical Geology 251, 120–127.
Reynard, B., Lécuyer, C., Grandjeau, P., 1999. Crystal-chemical controls on rare earth element concentrations in fossil biogenic apatite and implications for paleoenvironmental reconstructions. Chemical Geology 155, 233–242.
Riding, R., 2002. Structure and composition of organic reefs and carbonate mud mounds: concepts and categories. Earth Science Reviews 58, 163–231.
Rongemaille, E., Bayon, G., Pierre, C., Bollinger, C., Chu, N.C., Fouquet, Y., Riboulot, V., Voisset, M., 2011. Rare earth elements in cold seep carbonates from the Niger delta. Chemical Geology 286, 196–206.
Said, I., Somerville, I.D., Rodríguez, S., Cózar, P., 2013. Mississippian coral assemblages from the Khenifra area, Central Morocco: biostratigraphy, biofacies, palaeoecology and palaeobiogeography. Gondwana Research 23, 367–379.
Sartenaer, P., 1994. *Canavirila*, nouveau genre calvinariide (Rhynchonellide, Brachiopode) de la partie moyenne du Frasnien. Bulletin de l'Institut Royal des Sciences Naturelles de Belgique: Sciences de la Terre 64, 97–108.
Schlager, W., 2003. Benthic carbonate factories of the Phanerozoic. International Journal of Earth Sciences 92, 445–464.
Shields, G., Webb, G., 2004. Has the REE composition of seawater changed over geological time? Chemical Geology 204, 103–107.
Sommer, S.E., 1972. Cathodoluminescence of carbonates, 2. Geological applications. Chemical Geology 9, 275–284.
Stampfli, G.M., Borel, G.D., 2002. A plate tectonic model for the Paleozoic and Mesozoic constrained by dynamic plate boundaries and restored synthetic oceanic isochrones. Earth and Planetary Science Letters 196, 17–33.
Taylor, S.R., McLennan, S.M., 1985. The Continental Crust: Its Composition and Evolution. Blackwell Scientific Pub, Palo Alto (CA) 328 pp.
Tessitore, L., Schemm-Gregory, M., Korn, D., Wild, F.R.W.P., Naglik, C., Klug, C., 2012. Taphonomy and palaeoecology of the green Devonian gypidulid brachiopods from the AeM, eastern Anti-Atlas, Morocco. Swiss Journal of Palaeontology 132, 23–44.
Van Kranendonk, M.J., Webb, G.E., Kamber, B.S., 2003. Geological and trace element evidence for a marine sedimentary environment of deposition and biogenicity of 3.45 Ga stromatolitic carbonates in the Pilbara Craton, and support for a reducing Archaean ocean. Geobiology 1, 91–108.
Webb, G.E., Kamber, B.S., 2000. Rare earth elements in Holocene reefal microbialites: a new shallow seawater proxy. Geochimica et Cosmochimica Acta 64, 1557–1565. Webb, G.E., Nothdurft, L.D., Kamber, B.S., Kloprogge, J.T., Zhao, J.-X., 2009. Rare earth element geochemistry of scleractinian coral skeleton during meteoric diagenesis: a sequence through neomorphism of aragonite to calcite. Sedimentology 56, 1433–1463.
Wendt, J., 1985. Disintegration of the continental margin of northwestern Gondwana: Late Devonian of the eastern Anti-Atlas (Morocco). Geology 13, 815–818.
Wendt, J., 1993. Steep-sided carbonate mud mounds in the Middle Devonian of the eastern Anti-Atlas, Morocco. Geological Magazine 130, 69–83.
Wendt, J., Kaufmann, B., 2006. Middle Devonian (Givetian) coral-stromatoporoid reefs in West Sahara (Morocco). Journal of African Earth Sciences 44, 339–350.
Wendt, J., Bełka, Z., Moussine-Pouchkine, A., 1993. New architectures of deep-water carbonate buildups: evolution of mud mounds into mud ridges (Middle Devonian, Algerian Sahara). Geology 21, 723–726.
Wendt, J., Bełka, Z., Kaufmann, B., Kostrewa, R., Hayer, J., 1997. The world's most spectacular carbonate mud mounds (Middle Devonian, Algerian Sahara). Journal of Sedimentary Research 67, 424–436.
Zhang, J., Nozaki, Y., 1998. Behavior of rare earth elements in seawater at the ocean margin: a study along the slopes of the Sagami and Nankai troughs near Japan. Geochimica et Cosmochimica Acta 62, 1307–1317.